Geological Society of America Bulletin

Chronology of tectonic, geomorphic, and volcanic interactions and the tempo of fault slip near Little Lake, California

Colin B. Amos, Sarah J. Brownlee, Dylan H. Rood, G. Burch Fisher, Roland Bürgmann, Paul R. Renne and Angela S. Jayko

Geological Society of America Bulletin 2013;125, no. 7-8;1187-1202
doi: 10.1130/B30803.1

Notes

Chronology of tectonic, geomorphic, and volcanic interactions and the tempo of fault slip near Little Lake, California

Colin B. Amos[1,†], Sarah J. Brownlee[2], Dylan H. Rood[3,4], G. Burch Fisher[5], Roland Bürgmann[6], Paul R. Renne[7], and Angela S. Jayko[8]

[1]*Geology Department, Western Washington University, Bellingham, Washington 98225, USA*
[2]*Department of Geology, Wayne State University, Detroit, Michigan 48202, USA*
[3]*Accelerator Mass Spectrometry Laboratory, Scottish Universities Environmental Research Centre (SUERC), East Kilbride G75 0QF, UK*
[4]*Earth Research Institute, University of California, Santa Barbara, California 93106, USA*
[5]*Department of Earth Science, University of California, Santa Barbara, California 93106, USA*
[6]*Department of Earth and Planetary Science, University of California, Berkeley, California 94720, USA*
[7]*Berkeley Geochronology Center, Berkeley, California 94709, USA*
[8]*U.S. Geological Survey, U.C. White Mountain Research Station, Bishop, California 93514, USA*

ABSTRACT

New geochronologic and geomorphic constraints on the Little Lake fault in the Eastern California shear zone reveal steady, modest rates of dextral slip during and since the mid-to-late Pleistocene. We focus on a suite of offset fluvial landforms in the Pleistocene Owens River channel that formed in response to periodic interaction with nearby basalt flows, thereby recording displacement over multiple time intervals. Overlap between $^{40}Ar/^{39}Ar$ ages for the youngest intracanyon basalt flow and ^{10}Be surface exposure dating of downstream terrace surfaces suggests widespread channel incision during a prominent outburst flood through the Little Lake channel at ca. 64 ka. Older basalt flows flanking the upper and lower canyon margins indicate localization of the Owens River in its current position between 212 ± 14 and 197 ± 11 ka. Coupled with terrestrial light detection and ranging (lidar) and digital topographic measurements of dextral offset, the revised Little Lake chronology indicates average dextral slip rates of at least ~0.6–0.7 mm/yr and <1.3 mm/yr over intervals ranging from ~10^4 to 10^5 yr. Despite previous geodetic observations of relatively rapid interseismic strain along the Little Lake fault, we find no evidence for sustained temporal fluctuations in slip rates over multiple earthquake cycles. Instead, our results indicate that accelerated fault loading may be transient over much shorter periods (~10^1 yr) and perhaps indicative of time-dependent seismic hazard associated with Eastern California shear zone faults.

†E-mail: Colin.Amos@wwu.edu

INTRODUCTION

A comprehensive picture of the evolution and dynamics of plate-boundary deformation requires an inventory of geologic strain spanning intervals between 10^1 and 10^7 yr. Integrated over the entire deforming zone, time-averaged geologic strain equals the total rate of modern plate motion (DeMets et al., 2010). Deviations from this summed rate for networks of plate-boundary faults contain information about time-dependent, shear-zone processes (e.g., Friedrich et al., 2003; Oskin et al., 2008), progressive organization of a multifault array (Reheis and Dixon, 1996; Frankel et al., 2011), or the distribution of off-fault deformation (Shelef and Oskin, 2010). Accordingly, comparisons between short-term geodetic measurements of interseismic strain and longer-term geologic fault-slip rates afford insight into the dynamics of shear-zone evolution and the earthquake cycle (Dixon et al., 2003; Meade and Hager, 2005; Chuang and Johnson, 2011).

Such comparisons in the Eastern California shear zone (Fig. 1) have shed light on the rate, timing, and distribution of dextral shear in an evolving intracontinental plate-boundary fault system (e.g., Oskin and Iriondo, 2004; Frankel et al., 2011). Taken together, studies documenting present-day strain in eastern California from geodetic data (Savage et al., 1990; Argus and Gordon, 1991; Sauber et al., 1994; Hearn and Humphreys, 1998; Gan et al., 2000; McClusky et al., 2001; Miller et al., 2001; Bennett et al., 2003) reveal generally faster rates of interseismic deformation than that suggested by fault-slip rates measured from displaced Quaternary landforms (Reheis and Sawyer, 1997; Lee et al., 2001; Oskin and Iriondo, 2004; Bacon et al., 2005; Kirby et al., 2006; Frankel et al., 2007a, 2007b, 2011; Oskin et al., 2007; Kirby et al., 2008). This discrepancy between geodetic and geologic observations persists across the width of the deforming zone as a whole (Oskin et al., 2008) and also for individual faults within the array. In the northern Mojave Desert area, satellite radar interferometry measurements spanning 1992–2000 (Peltzer et al., 2001) indicate that much of the current strain accumulation occurs along the Little Lake and Blackwater faults (Fig. 1), despite modest Quaternary slip rates for these structures (Roquemore, 1980; Oskin and Iriondo, 2004). Notably, the sinistral Garlock fault, which crosscuts this apparent shear zone, exhibits Holocene–late Pleistocene slip rates that exceed modern interseismic strain by an approximate factor of 2–3 (McGill et al., 2009; Ganev et al., 2012). It remains unknown whether these discrepancies reflect short-lived transients in the geodetic data or persist over multiple earthquake cycles (~10^2–10^3 yr).

This question bears strongly on our understanding of the distribution and timing of strain release during large earthquakes in the Eastern California shear zone. One possibility holds that the conjugate Little Lake–Blackwater and Garlock faults undergo alternating periods of relatively slow and fast slip (Peltzer et al., 2001; Dolan et al., 2007), corresponding with earthquake clusters along each zone (Rockwell et al., 2000; Dawson et al., 2003). In this scenario, feedbacks between earthquake slip and the transient strength of underlying ductile shear zones may give rise to currently increased rates of loading along Eastern California shear zone faults (Oskin et al., 2008). If so, the nature and persistence of short- and long-term variations in fault-slip rate for these structures provide insight into the

GSA Bulletin; July/August 2013; v. 125; no. 7/8; p. 1187–1202; doi: 10.1130/B30803.1; 9 figures; 2 tables; Data Repository item 2013227.

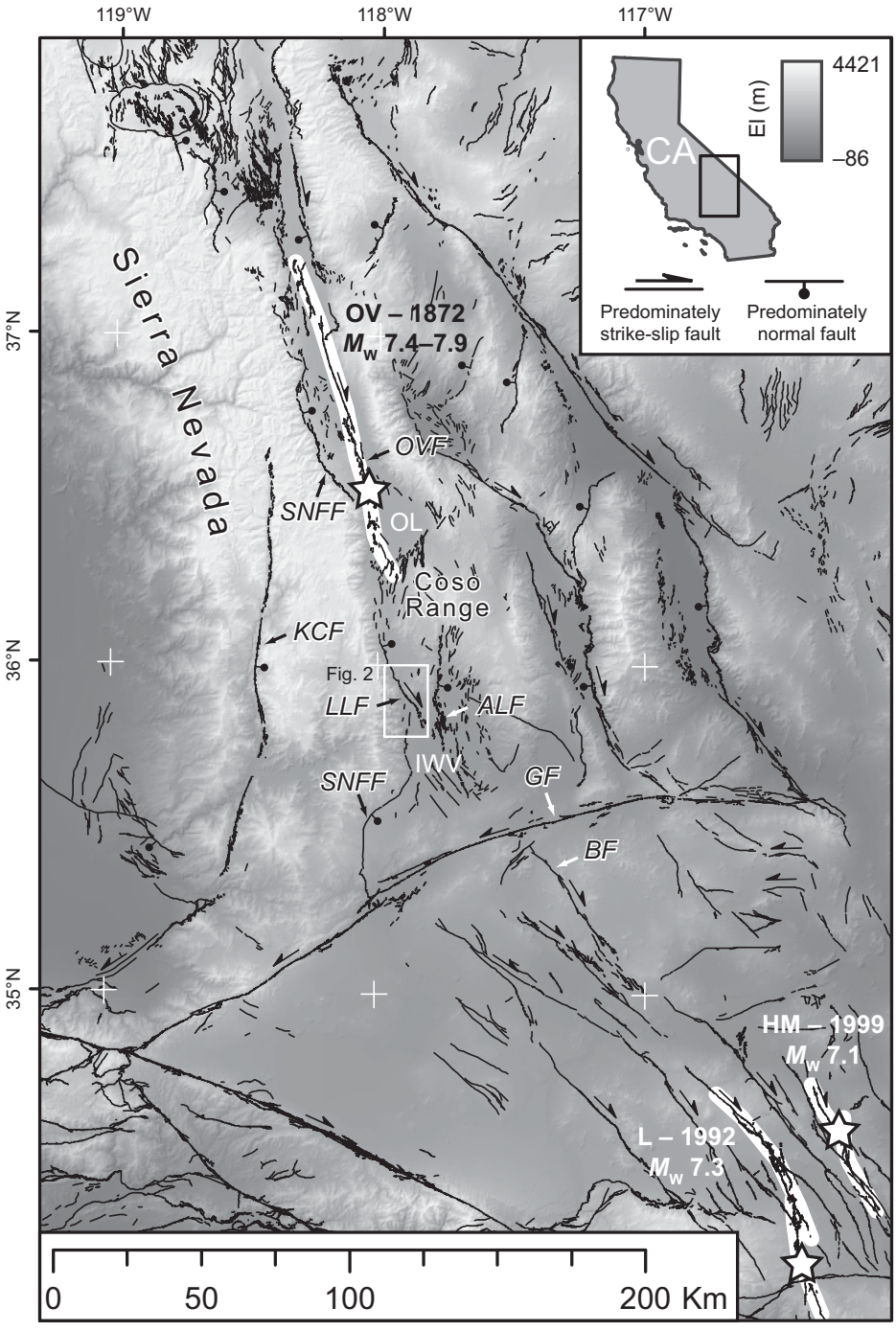

Figure 1. Overview of active faults and regional topography of the Eastern California shear zone (ECSZ) and southern Walker Lane belt. Labeled faults are abbreviated as follows: ALF—Airport Lake fault, BF—Blackwater fault, GF—Garlock fault, KCF—Kern Canyon fault, LLF—Little Lake fault, OVF—Owens Valley fault, SNFF—Sierra Nevada frontal fault. OL—Owens Lake, IWV—Indian Wells Valley. Major historical earthquake surface ruptures in the Eastern California shear zone and Walker Lane belt are outlined in white, with stars denoting epicentral locations: OV—1872 Owens Valley, L—Landers 1992, HM—1999 Hector Mine. Active fault traces are taken from the U.S. Geological Survey Quaternary fault and fold database, with the exception of the Kern Canyon fault, taken from Brossy et al. (2012).

potential time dependence of seismic hazards in southeastern California (Petersen et al., 2007).

In this paper, we test whether relatively rapid interseismic shear in the Eastern California shear zone manifests as fluctuations in fault-slip rate during the late Pleistocene. We focus on the Little Lake fault, which forms the western boundary of the Eastern California shear zone north of the Garlock fault (Fig. 1), and which lies along the northward continuation of the pronounced velocity discontinuity imaged from satellite radar (Peltzer et al., 2001). There, we capitalize on a set of previously undescribed landforms reflecting repeated drainage of the Pleistocene Owens River through the Little Lake area. Surficial mapping, terrestrial laser scanning (TLS), and ^{10}Be exposure dating of these surfaces, combined with ^{40}Ar/^{39}Ar constraints on young, intervening lava flows, provide the first geologic slip rates for the Little Lake fault based on high-quality geochronologic data. Our results also inform the history and timing of pluvial drainage in the Pleistocene Owens River system and illustrate the impact of volcanic eruptions on channel localization and terrace development. Taken together, these new data bridge a critical temporal gap (~10^4–10^5 yr) in our understanding of the way in which active strain and earthquakes evolve and are partitioned within the Eastern California shear zone.

LITTLE LAKE FAULT

The Little Lake fault is part of a distributed network of dextral, normal, and dextral-oblique faults east of the Sierra Nevada in California and Nevada that together constitute the Eastern California shear zone (Dokka and Travis, 1990) or southern Walker Lane belt (Stewart, 1988; Wesnousky, 2005) (Fig. 1). Geodetic observations over the past several decades reveal that this ~100–150-km-wide zone accommodates roughly one-quarter (~12 ± 2 mm/yr) of the total relative motion between the Pacific and North American plates (~50 mm/yr) (e.g., Bennett et al., 2003). At ~36°N latitude (Fig. 1), the Little Lake fault separates the western margin of this deforming zone from the southeastern corner of the relatively stable Sierra Nevada block (Dixon et al., 2000). Active extension in this portion of the Eastern California shear zone occurs mainly in association with releasing stepovers between dextral faults (Unruh et al., 2003). Together with the right-oblique Owens Valley fault to the north, the dextral Little Lake fault forms an extensional relay across the Coso Range (Fig. 1), resulting in focused extension, crustal thinning, geothermal activity, and abundant shallow seismicity (Unruh et al., 2002; Monastero et al., 2005).

Southward toward the Garlock fault, the Little Lake and normal Airport Lake faults merge into a single, albeit highly segmented, NW-striking shear zone that cuts the relatively low-relief basin surface of the Indian Wells Valley (Figs. 1 and 2). Several recent earthquakes near this intersection, including the 1982 M 5.2 Indian Wells Valley and the 1995 M 5.8 and 5.4 Ridgecrest events, produced modest, en echelon ground cracking along a northwestern trend (Roquemore and Zellmer, 1983; Hauksson et al., 1995). Constraints on earlier earthquakes along the Little Lake fault come from radiocarbon dating of trench deposits that limit the most recent surface rupture to younger than ca. 2.5 ka (Roquemore, 1981). Although structurally discontinuous across the Garlock fault, the Little Lake and Blackwater structures occupy an apparent gap between large historical surface ruptures of the 1872 Owens Valley and 1992 Landers earthquakes (Fig. 1) (Peltzer et al., 2001).

The most prominent surface expression of the Little Lake fault occurs near the intersection of the western Coso Range and Sierra Nevada to the west. There, the fault cuts a series of Quaternary basalt flows emanating from local volcanic centers, as well as older alluvial deposits shed from the adjacent Sierra Nevada range front (Fig. 2). Relatively continuous segments of the Little Lake fault define an overall arcuate geometry, smoothly transitioning toward more northwesterly orientations before terminating into a series of nearly perpendicular normal fault splays to the southeast (Roquemore, 1980). Vertical offset of the intact basalt flow top in this location is limited to these extensional relays and localized pull-apart basins, demonstrating nearly pure dextral motion along the Little Lake fault.

At its northwestern end, segments of the Little Lake fault terminate beneath younger alluvial-fan deposits in Rose Valley, and/or merge with the Sierra Nevada frontal faults to the west (Fig. 2). Relatively short, disrupted drainages along this portion of the southeastern Sierra Nevada range front suggest that some component of dextral slip is transferred onto these normal faults, consistent with similar geomorphic evidence in northwestern Rose Valley (Wills, 1989; Amos et al., 2013). Although complicated by relatively chaotic landslide blocks from the Sierra Nevada to the southwest, steeply dipping panels of older alluvial deposits suggest either tilting or folding across a restraining left step between these oblique range-front structures and the Little Lake fault. Well-preserved fault geomorphology in the Little Lake area (Fig. 3) also preserves features such as shutter ridges, side-hill benches, linear troughs and springs, and pressure ridges along the fault zone (Fig. 4) (Duffield and Smith, 1978a; Roquemore, 1980).

QUATERNARY GEOLOGY OF THE LITTLE LAKE AREA

The Little Lake fault straddles the geomorphic and physiographic boundary between Rose Valley to the north and Indian Wells Valley to the south (Fig. 2). Since at least the mid-Pleistocene, the ~150-m-deep canyon separating these two valleys, herein referred to as Little Lake narrows (Fig. 2), has funneled overflow from the Owens Lake basin to the China Lake and Searles Lake basins during pluvial lake highstands (Duffield and Smith, 1978a, 1978b). These lake basins were part of a larger chain of variably interconnected Pleistocene lakes in the western Great Basin that ultimately linked drainage in the Mono Basin in the north with Death Valley in the southeast (Gale, 1914; Blackwelder, 1933; Smith and Street-Perrott, 1983; Jannik et al., 1991). Phillips (2008) summarizes the geologic and hydrologic conditions within the paleo–Owens River drainage system since the mid-Tertiary.

Little Lake itself represents a small, natural, spring-fed lake situated within an inset channel cut at the upper end of Little Lake narrows (Fig. 3). Coring and radiocarbon dating indicate saltgrass meadow or freshwater marsh deposition between ca. 3000 and 5000 radiocarbon yr B.P., and persistence of a shallow freshwater lake over the past ~3000 radiocarbon years (Mehringer and Sheppard, 1978). Young, coalescing alluvial fans form a natural dam at the southern end of the lake (Fig. 3), and Mehringer and Sheppard (1978) indicated maximum water depths up to 2 m.

Volcanic Rocks

Local basaltic eruptions have profoundly impacted the position of the Pleistocene Owens River channel and the geomorphic development of Little Lake narrows. Interactions between volcanism and Owens River drainage were first recognized and described in detail by Duffield and Smith (1978a, 1978b) based on mapping and potassium-argon (K-Ar) dating later published as Duffield et al. (1980) and Duffield and Bacon (1981), respectively. These authors recognized that eruption of two stacked basalt flows (Qb1) from a cinder cone along the Little Lake fault onto older, SE-sloping alluvial fans (Qfo) (Fig. 2) clearly predated localization of the river channel in its current position. These flows are moderately porphyritic, and Duffield and Smith (1978a) reported between 10% and 20% phenocrysts up to 3 mm in size, predominately consisting of plagioclase, with lesser altered olivine and clinopyroxene. Beds of deeply weathered alluvial-fan boulders and gravel currently rest beneath Qb1 flows on the ~150-m-high eastern canyon wall, attesting to their former continuity with fan remnants flanking the Sierra Nevada range front to the west (Fig. 4A). Duffield and Smith (1978a) also indicated that the lack of an intervening soil between these the upper and lower units suggests a similar eruptive age for both flows.

The absence of alluvial deposits on top of the Qb1 basalt flows may imply that establishment of the channel and downcutting through Little Lake narrows occurred shortly after eruption of the upper Qb1 flow. K-Ar ages from the upper and lower flows (399 ± 45 ka and 486 ± 108 ka, respectively; Duffield et al., 1980) provide maximum bounds on the age of this event (Duffield and Smith, 1978a). Based on gravity and magnetic data, these authors also recognized a former course of the Owens River ~5 km to the east, now buried by Pleistocene lavas and sediment (Fig. 2).

Two younger, intracanyon basalt flows (Qb2 and Qb3) postdate establishment of the Owens River channel through the Little Lake area. The older of these flows (Qb2) emanated from an eroded cinder cone within the Coso Range and flowed at least ~15 km downstream upon entering Little Lake narrows (Duffield and Bacon (1981) (Fig. 2). The Qb2 lava contains only a few percent phenocrysts of olivine and plagioclase up to ~1–2 mm, and is thus readily differentiated from the Qb1 basalt (Duffield and Smith, 1978a). The Qb2 flow is at least ~70 m thick immediately east of Little Lake, where cliff exposures reveal pervasive and well-developed columnar jointing (Fig. 3). Based on this thickness, the Qb2 lava likely overwhelmed the Owens River channel, although no erosional remnants of this flow are present along the western canyon wall. Nevertheless, the Owens River subsequently reestablished its course through Little Lake sometime before eruption of the younger Qb3 flow. Low levels of radiogenic argon for Qb2 led to an imprecise K-Ar age of 140 ± 89 ka reported by Duffield et al. (1980), although younger pyroclastic deposits blanketing the Qbc2 cone indicate a minimum K-Ar age of 77 ± 8 ka (Lanphere et al., 1975).

The youngest intracanyon lava flow at Little Lake (Qb3), termed the basalt of Red Hill by Duffield and Smith (1978a) after the prominent ~180-m-high cinder cone at the southern end of Rose Valley, also exploited the Owens River channel and flowed ~16 km downstream (Fig. 2). Duffield and Smith (1978a) reported a modal abundance for the Qb3 flow of up to

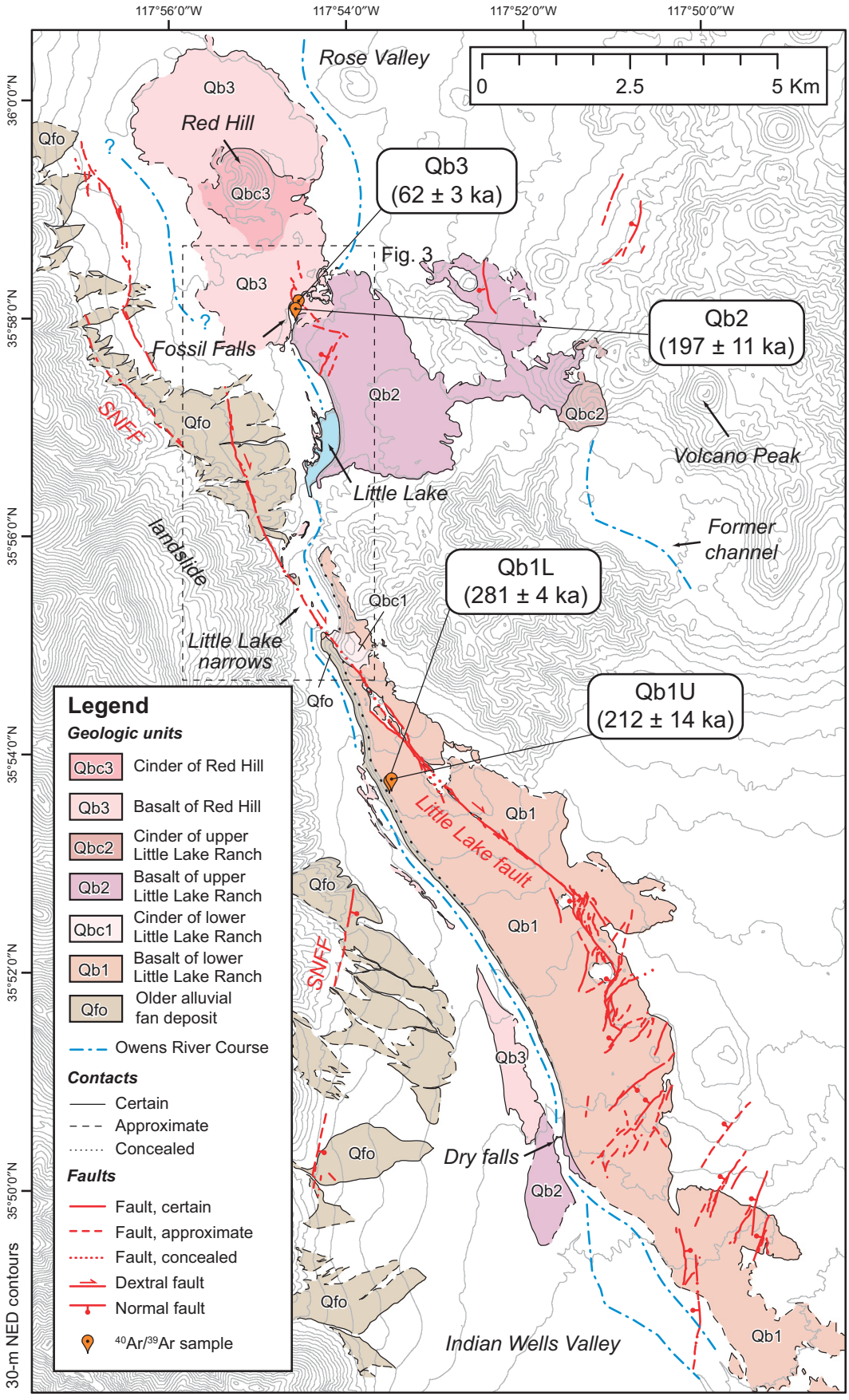

Figure 2. Simplified geologic map of the Little Lake fault, highlighting Quaternary volcanic and alluvial deposits bearing on the Pleistocene drainage of Owens River through the Little Lake area. Map units are named and modified from Duffield and Bacon (1981). The 30 m elevation contours are taken from the National Elevation Database (NED). The $^{40}Ar/^{39}Ar$ dates are labeled as in Table 1. SNFF—Sierra Nevada frontal fault.

Figure 3 (*legend on following page*). Quaternary surficial geologic map of the upper Little Lake narrows and Fossil Falls areas. Volcanic map units are modified from Duffield and Bacon (1981). The 10 m elevation contours are taken from the National Elevation Database (NED). The map location is shown by the boxed area in Figure 2. Yellow and brown circles indicate sample locations for $^{40}Ar/^{39}Ar$ and ^{10}Be dating, respectively.

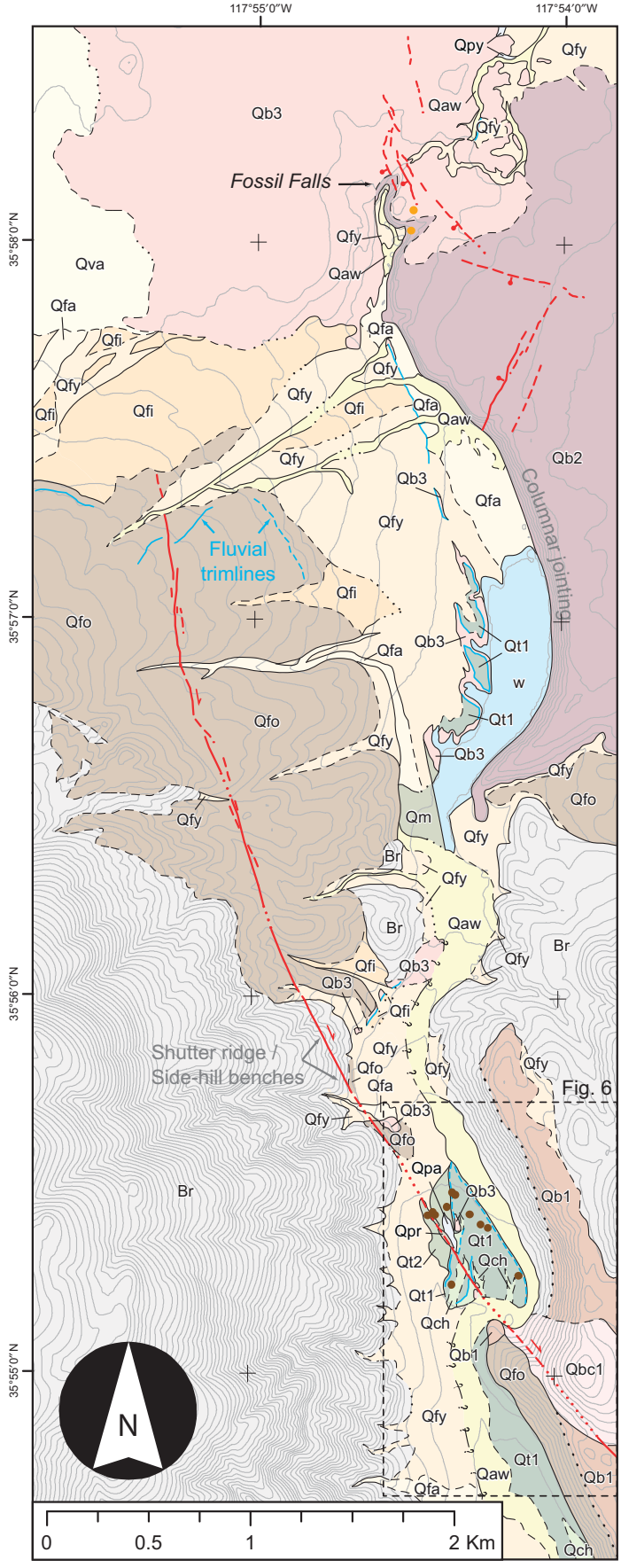

10%–20% plagioclase, olivine, and clinopyroxene phenocrysts up to 3 mm in size. They also noted the similarity between this flow and the upper Qb1 lavas, although the position of the Qb3 flow within the Little Lake narrows enables easy distinction from the relatively weathered Qb1 flow atop the canyon margins. Rough and ropy flow tops distinguish largely uneroded portions of the Qb3 flow at Red Hill and farther downstream, where intact Qb3 lava lies in depositional contact with the underlying Qb2 flow (Duffield and Bacon, 1981) (Fig. 2). Within the Little Lake channel, however, remnants of Qb3 form eroded, planar bedrock surfaces or straths underlying a veneer of bouldery alluvium. This surface is readily visible beneath the overlying terrace cover along the canyon floor, where repeated slip has warped and broken the originally planar basalt strath into a prominent pressure ridge along the Little Lake fault (Fig. 4B). Isolated erosional remnants of the Qb3 flow are also present within Little Lake narrows, flanking the western inner rim of the canyon wall (Fig. 3). Original attempts to date the basalt of Red Hill using K-Ar failed due to insufficient radiogenic argon (Duffield and Smith, 1978a), although early application of ^{3}He surface exposure dating yielded an age of ca. 57–62 ka for the flow top (Cerling, 1990).

Geomorphology

Landforms and deposits reflecting repeated scour by the Pleistocene Owens River through Little Lake narrows are superimposed on the Little Lake basalts and older alluvial gravels (Fig. 3). Impacts of this intermittent drainage are immediately apparent as a series of stepped, dry waterfalls along the former river course. The northernmost of these cascades, Fossil Falls, drops ~30 m over two distinct steps localized along a series of normal fault scarps cutting the Qb3 flow top (Fig. 3). These faults also control the position of a second, amphitheater-shaped dry falls that connects with Fossil Falls to the west via a series of dry erosional channels. Within Fossil Falls, remarkable fluvial scour,

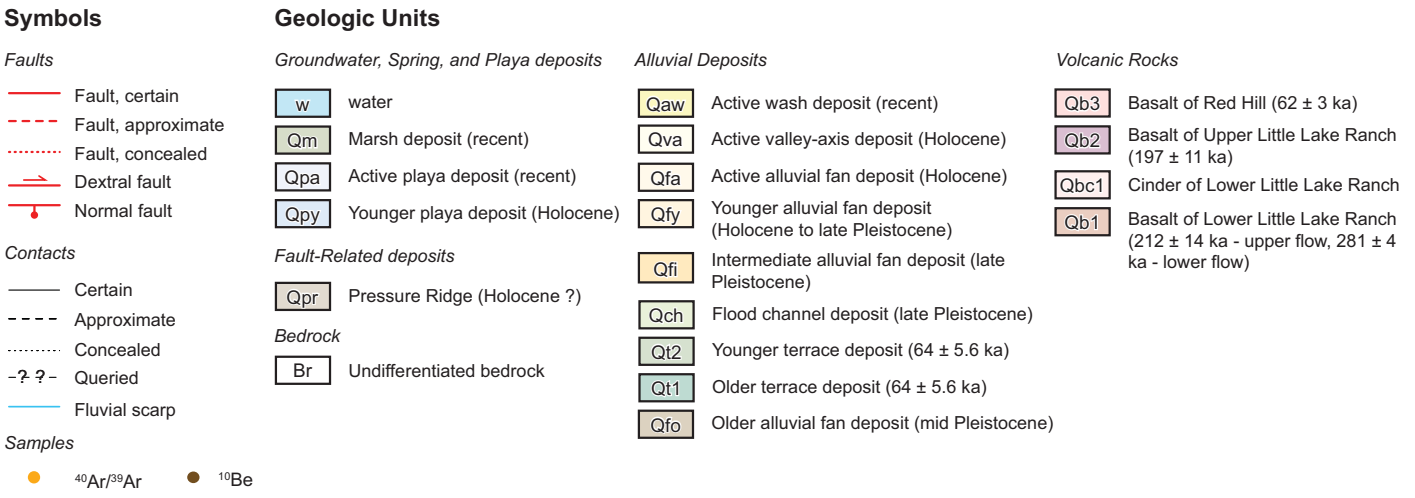

Figure 3 (*legend*).

polish, and meter-scale potholes developed on the Qb3 basalt attest to the scale of this outflow (Saint-Amand, 1987). A smaller, ~5 m step in the channel profile occurs in the northern Indian Wells Valley, where the Owens River crosses the Qb2 lava at its downstream extent (Dry Falls, Fig. 2). Earlier ^{3}He surface exposure dating of polished basalt at Fossil Falls suggests that the most recent scour occurred at ca. 16–17 ka (Cerling, 1990).

At least two generations of fluvial terraces and inset channels mark the course of the former Owens River between Fossil Falls and northern Indian Wells Valley. Within Little Lake narrows, these terraces consist of a somewhat discontinuous and patchy suite of surfaces flanking the modern wash and resting above the modern lake surface (Fig. 3). Terrace cover sediments contain boulders up to several meters in diameter deposited on a prominent strath cut within Qb3 basalt flooring Little Lake narrows. These clasts are largely derived from the Qb3 basalt but also contain ~10% felsic plutonic rocks. Potential origins for these rocks include either quartz monzodiorite or alkali-feldspar granite exposed along the eastern wall of Little Lake narrows (Whitmarsh, 1998) or upstream granitic sources in the Sierra Nevada.

Where juxtaposed in Little Lake narrows (Fig. 4B), older terrace treads (Qt1) lie ~3–5 m above a younger, inset surface (Qt2), separated by a narrow terrace riser. The lower Qt2 terrace exposes the underlying basalt strath along its western edge beneath somewhat patchy and partially stripped cover sediments. Where these surfaces intersect the Little Lake fault (Fig. 4B), this strath projects beneath the bouldery Qt1 cover, indicating that Qt2 may represent a cut terrace inset within several meters of Qt1 fill. The strath underlying Qt1 is readily visible at the upper end of the narrows, where isolated terrace remnants flank the western edge of the modern wash now occupied by the modern Little Lake (Fig. 3). Remnants of the Qt1 surface not buried by younger alluvial fans are modified by a series of inset channels creating surface relief on the order of several meters. Although some of these channels grade downstream to the modern wash or lake level, they are either buried by younger alluvial fans at their upstream end or are isolated from the active wash by terrace risers up to ~5 m high (Figs. 3 and 4B).

QUANTIFYING FAULT OFFSET WITH TERRESTRIAL LIDAR

Landforms within the Pleistocene Owens River channel serve as robust geomorphic markers of dextral slip along the Little Lake fault. Greater offset of older landscape features indicates ongoing deformation and provides a measure of displacement integrated over varying time intervals. Traditionally, quantifying such offsets along strike-slip faults relies on map-view projection of offset linear features (e.g., stream channels) onto the fault surface trace (Wallace, 1968). Reported uncertainties in this approach typically encompass a somewhat subjective range based on the projection geometry or the preservation integrity of the offset geomorphic feature. With increasing availability and usage of digital topography, specifically, light detection and ranging (lidar) data, lateral offset measurements now commonly rely on more three-dimensional topographic and geomorphic reconstructions (e.g., Zielke and Arrowsmith, 2012). As such, we adopted an approach using serial topographic profiles to measure the actual range of permissible offsets for each feature. This method presents the distinct advantage of creating individual probability distributions of displacement for each feature used in subsequent slip-rate calculations.

The faulted Qt1-Qt2 terrace riser within Little Lake narrows provides the best surface expression of dextral offset along the Little Lake fault (Fig. 5). Initial reconnaissance of this feature using Google Earth imagery suggested lateral offset between 33 and 37 m, with a nominal uncertainty of ±10 m, reflecting the map-view riser width. Subsequently, we completed a terrestrial laser scanning (TLS) survey to refine this measurement from detailed topographic reconstructions of the faulted riser geometry (Fisher et al., 2012). Several studies have highlighted the utility of portable TLS for characterizing fault displacement in areas without airborne lidar coverage (Oldow and Singleton, 2008; Gold et al., 2009, 2011) or for applications requiring high-density point cloud data (Gold et al., 2012). TLS surveying utilized a Riegl LMS-Z420i ground-based lidar system, resulting in collection of ~22 million individual laser returns at an average density of 20 points/m^2. Nonground returns from sparse brush covering the area were filtered using the Terrasolid software package, and the remaining returns were triangulated to create an equally spaced digital elevation model (DEM) at a nominal resolution of 50 cm (Fig. 5A) (cf. Perroy et al., 2010).

Serial elevation profiles with 2 m point spacing were extracted from the resulting DEM along the western terrace riser (Fig. 5B) and the incised eastern edge of the Qt1 terrace (Fig. 5C). Profile elevations were then projected perpendicular to the average local riser orientation on either side of the fault. As a group, profiles were then projected into a coordinate system normal to the local fault strike in order to reconstruct the total dextral displacement of each feature. This reconstruction

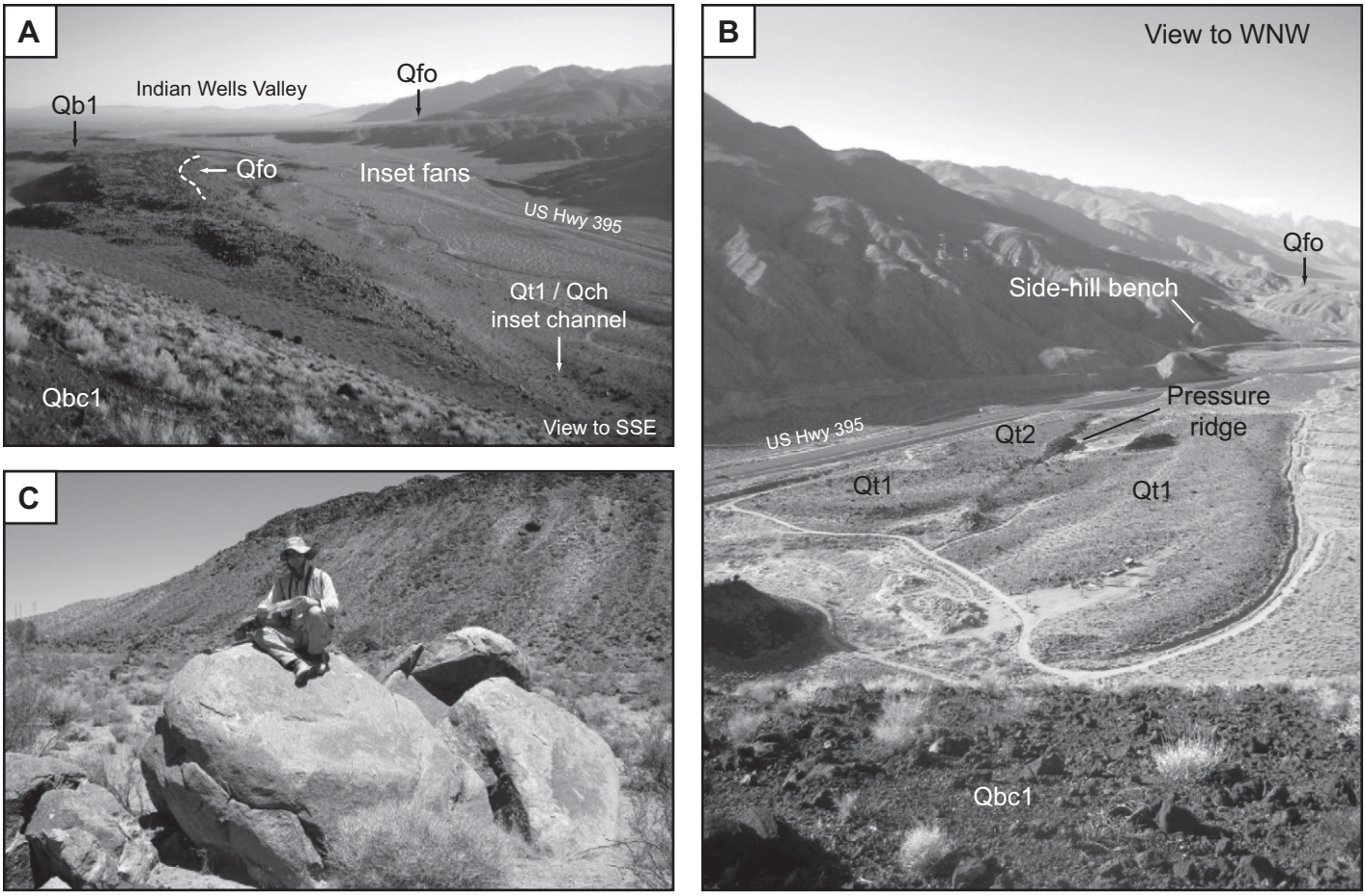

Figure 4. Field photographs of (A) the lower Little Lake narrows and Owens River channel draining south toward Indian Wells Valley, (B) offset terraces and other tectonic geomorphic features along the Little Lake fault, and (C) sampled boulder LL-Qt1–01 for ^{10}Be surface exposure dating. Geologic units are labeled as in Figures 2 and 3.

utilized the distance range between topographic midpoints from the scarp profiles on either side of the fault (Figs. 5B and 5C), based on the assumption that the scarp midpoint undergoes the least amount of vertical change during scarp diffusion (Pelletier et al., 2006).

Measured lateral displacement of the Qt1 terrace edge ranges between 30 and 42 m and 34 and 49 m for the western and eastern margins, respectively (Figs. 5B and 5C). These measurements incorporate the maximum and minimum distance range of riser midpoints grouped on either side of the fault. Given the local linearity and continuity of each riser segment, as well as the fault trace, uncertainty associated with projection of these features is smaller than the observed range of riser midpoints. These measurements compare favorably with estimates based on image reconstruction (Fisher et al., 2012) and present the distinct advantage of reflecting the actual range of permissible displacements based on the shape and integrity of the faulted terrace riser.

The eastern margin of Little Lake narrows also provides an offset marker for measuring displacement along the Little Lake fault (Fig. 3). Because our TLS survey was limited to the canyon floor, we employ a simple geometric restoration of the relatively steep, ~160-m-high cliff capped by Qb1 basalt (Fig. 6). At its base, this cliff coincides with a prominent deflection of the active wash, where progressive offset forces southward drainage around the cliff margin to the west. This deflection coincides with an isolated remnant of Qb1 just above the active wash on the southwest side of the fault. Reconstruction of the base of the canyon wall indicates at least ~140 m of dextral displacement, depending on how this feature is projected into the fault on its southwest side (Fig. 6B). We consider this estimate to represent a minimum value on the total offset given the potential for and likelihood of erosion along the base of the cliff, and its relatively oblique orientation relative to the Little Lake fault. Previous estimates by Roquemore (1980), based on geometric reconstruction of small pull-apart structures preserved on top of the Qb1 flow (Fig. 2), indicate somewhat higher offset values up to 250 m. Although somewhat obscured by the cinder cone atop the Qb1 surface, restoring 250 m of dextral slip along the Little Lake fault provides a reasonable match along the upper edge of the canyon wall (Fig. 6C). As such, we consider this value as a maximum bound on the total displacement of the eastern margin of Little Lake narrows.

^{40}Ar/^{39}Ar DATING

New, high-precision ^{40}Ar/^{39}Ar dating of Quaternary basalt flows revises the volcanic and geomorphic chronology at Little Lake and bears directly on the time-integrated slip history for the Little Lake fault. We collected samples from each of the three main flows at Little Lake, including the upper and lower flows of Qb1 (Fig. 2). The samples were crushed and sieved to 125–250 μm size fractions, and groundmass was separated using standard separation techniques

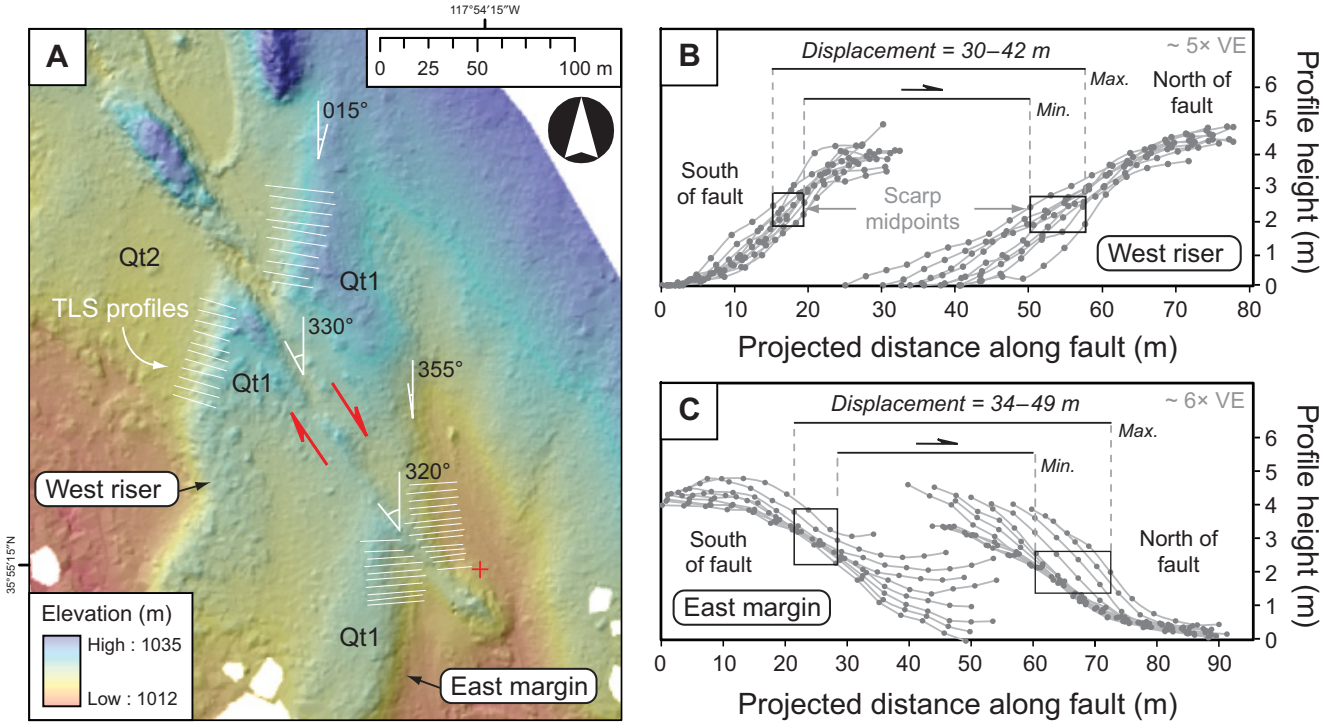

Figure 5. (A) 50 cm digital elevation model derived from terrestrial laser scanning (TLS) of displaced terrace risers in Little Lake narrows. (B–C) Stacked topographic profiles along the western and eastern edges of the Qt1 surface, respectively, used to reconstruct the total dextral offset of the Qt1-Qt2 terrace riser. Individual profiles were extracted perpendicular to the average riser orientation and were then projected onto a plane parallel to the local fault strike. Profile locations for each margin are shown in A. VE—vertical exaggeration.

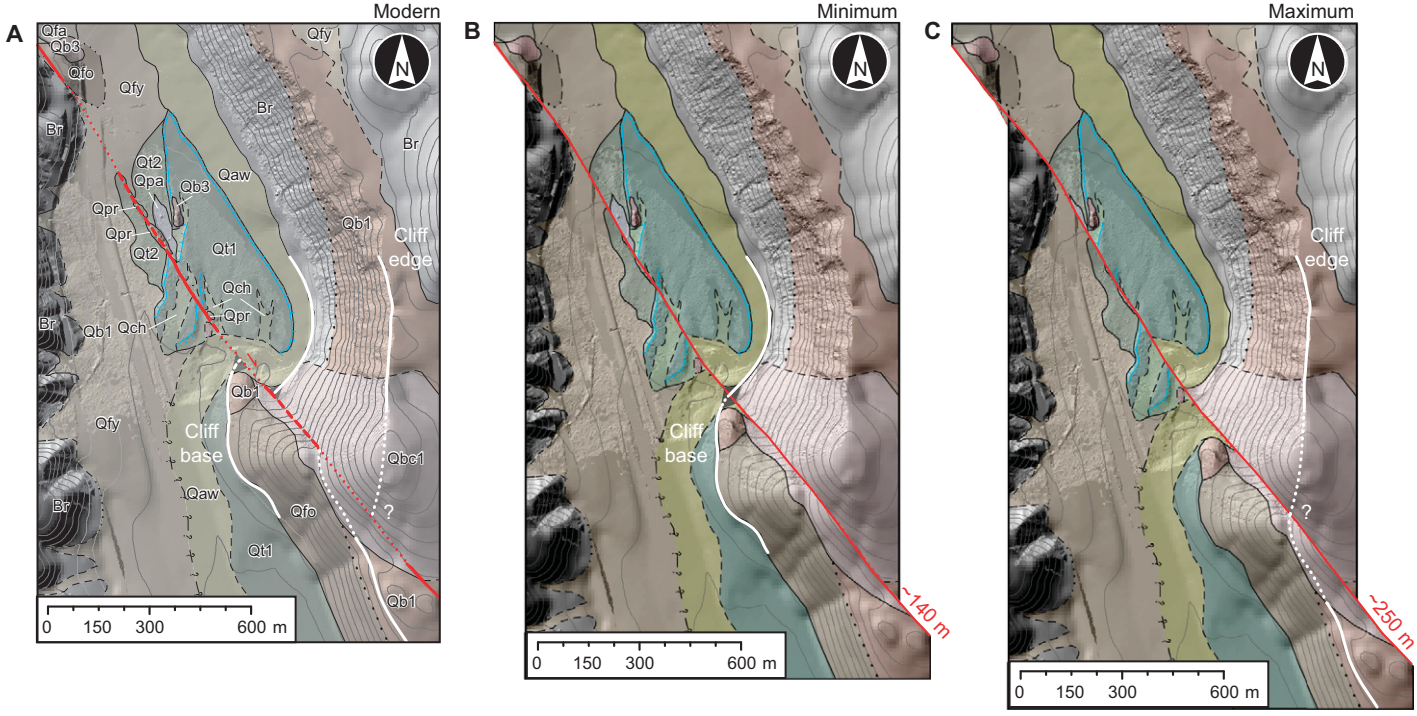

Figure 6. Geometric reconstruction of (A) the modern geomorphic configuration of the upper Little Lake narrows indicates between ~140 and 250 m of dextral offset for the base (B) and upper edge (C) of the eastern canyon wall. Geologic units are labeled as in Figure 3. The base image includes a hillshade image from our terrestrial laser scanning (TLS) survey, as well as 10 m contours overlain on a National Elevation Database (NED) hillshade map. The map location is shown by the boxed area in Figure 3. Geologic units are labeled as in Figures 2 and 3.

TABLE 1. $^{40}Ar/^{39}Ar$ SAMPLE LOCATIONS, STEP-HEATING RESULTS, AND COMBINED PLATEAU AGES

Sample	Lat./Long. (Decimal degrees)	Number of heating steps	Plateau age, ±1σ (ka)*	MSWD†	Probability
Qb1U-1	35.8949°, –117.8904°	13	217 ± 19	0.74	0.71
Qb1U-2	–	14	205 ± 21	0.76	0.70
Qb1U combined	–	27	212 ± 14	0.73	0.84
Qb1L-1	35.8948°, –117.8905°	14	278 ± 6	0.51	0.92
Qb1L-2	–	14	285 ± 6	0.36	0.98
Qb1L combined	–	28	281 ± 4	0.44	0.99
Qb2-1	35.9670°, –117.9090°	14	199 ± 15	0.19	0.999
Qb2-2	–	14	195 ± 18	0.25	0.997
Qb2 combined	–	28	197 ± 11	0.21	0.999
Qb3-1	35.9682°, –117.9082°	14	64 ± 5	0.34	0.99
Qb3-2	–	14	61 ± 4	0.40	0.97
Qb3 combined	–	28	62 ± 3	0.36	0.998

*Plateau ages include all steps of each step-heating experiment, and combined ages include all steps from both aliquots of each sample. Errors reported are 1σ. Ages were calculated using the calibration of Renne et al. (2011). Data for each step-heating increment are included in supplemental data Table 1 (see text footnote 1).
†MSWD—mean square of weighted deviates.

combined with removal of phenocryst fragments by hand using a binocular microscope and tweezers. We used only groundmass for these basalts because (1) phenocrysts of plagioclase tend to be more calcium-rich than groundmass, and when dating basalts of such young age, it is important to minimize the corrections required for ^{40}Ar produced in neutron reactions on ^{40}Ca in the reactor, and (2) phenocrysts may host excess ^{40}Ar. The groundmass samples were loaded into irradiation disks with aliquots of Fish Canyon sanidine for use as a neutron-flux monitor, and irradiated for 30 min at the Oregon State Triga reactor. Ages were calculated using the calibration of Renne et al. (2011). We step-heated two aliquots of each sample in 13–14 steps using a CO_2 laser, and measured the gas released on a MAP 215 mass spectrometer by peak-hopping using a Balzer's electron multiplier in analog mode at the Berkeley Geochronology Center. Step-heating results are listed in Table 1, and Table DR1 [see footnote 1][1] and age spectra are plotted in Figure 7. Plateau ages were calculated as the inverse-variance weighted mean of plateau steps, which included all steps for all of these samples. The plateau ages from the two aliquots of each sample agreed with one another within 2σ, so we were able to combine the steps from each aliquot into one plateau age.

The new $^{40}Ar/^{39}Ar$ results mark a vast improvement on the precision and accuracy of previous endeavors to date these basalt flows, which used the K-Ar technique on whole-rock samples (Duffield et al., 1980). For the oldest flow, Qb1L (the lower unit of Qb1), we obtained a combined plateau age of 281 ± 4 (1σ) ka, which is a 20-fold improvement on the precision of 486 ± 108 ka reported in Duffield et al. (1980). For the next younger flow, Qb1U (upper unit of Qb1), we also obtained a younger age with better precision at 212 ± 14 ka (1σ), as compared to 399 ± 45 ka (Duffield et al., 1980). The calibration we used intrinsically yields ~2% older ages than that used by Duffield et al. (1980); thus, the younger ages we obtained are noteworthy. One possible explanation is that we used only groundmass rather than whole-rock samples, which may include phenocrysts that formed slightly before eruption or which may contain excess ^{40}Ar. For the next younger flow, Qb2, we obtained an age of 197 ± 11 ka, which lies within 1σ uncertainty of the previous result of 140 ± 89 ka. Again, we were able to achieve much higher precision than the previous study. For the youngest flow, Qb3, our age of 62 ± 3 ka agrees well with previous estimates of the eruption age (ca. 57–62 ka) based on ^{3}He exposure dating of the flow top (Cerling, 1990). Duffield et al. (1980) cited insufficient radiogenic argon, but by using only groundmass and the more precise and sensitive $^{40}Ar/^{39}Ar$ method, we were able to date this flow quite precisely.

^{10}Be EXPOSURE DATING

The ^{10}Be surface exposure dating of quartz-rich, felsic boulders on the Qt1 and Qt2 surfaces also yielded new constraints on landform age and late Pleistocene slip rates in Little Lake narrows. We collected and processed a total of 11 samples from the intact tops of large boulders preserved on terrace treads (Fig. 4C) in order to minimize the effects of postdepositional erosion, spallation, or boulder burial. Samples were collected using a hammer and chisel to remove the outer few centimeters of unbroken, indurated boulder rinds.

Quartz purification and ^{10}Be extraction were completed at Lawrence Livermore National Laboratory (LLNL). Quartz was separated and meteoric ^{10}Be removed using methods described by Kohl and Nishiizumi (1992). The Be carrier used at LLNL is a low-background carrier prepared from beryl with an ~8×10^{-16} $^{10}Be/^{9}Be$ ratio. After adding the Be carrier, quartz was dissolved in an HF/HNO_3 solution. The solution was dried down to remove Si as SiF_6, and fumed several times with $HClO_4$ to evaporate residual fluorides. Beryllium was separated using ion exchange column procedures similar to Stone (2004) with anion exchange using HCl and cation exchange using dilute H_2SO_4 and HCl (Ditchburn and Whitehead, 1994). Beryllium was then precipitated as beryllium hydroxide, ignited to beryllium oxide, mixed with niobium powder, and loaded into stainless-steel cathodes, prior to measurement.

The $^{10}Be/^{9}Be$ isotope ratios were measured at the Center for Accelerator Mass Spectrometry at LLNL (Rood et al., 2010, 2013). The process blank was 36,654 ± 11,051 ^{10}Be atoms, 0.9%–2.9% of the total number of ^{10}Be atoms in the samples. The 1σ analytical uncertainties for $^{10}Be/^{9}Be$ ratios were 1.9%–2.9%. Be isotope ratios were calibrated to the 07KNSTD3110 standard with a reported $^{10}Be/^{9}Be$ ratio of 2.85×10^{-12} described in Nishiizumi et al. (2007), which uses the revised nominal isotope ratio and ^{10}Be decay constant.

Surface exposure ages were calculated using the CRONUS-Earth online exposure age calculator, version 2.2 (constants version 2.2.1), as described in Balco et al. (2008) using a constant production rate model and the scaling scheme for spallation of Lal (1991) and Stone (2000). Model exposure ages were calculated using two erosion rate scenarios: (1) no boulder erosion, and (2) a nominal boulder erosion rate of 0.2 cm/k.y., designed to mimic measured erosion rates from similar alluvial-fan boulders in Owens Valley, ~100 km to the north (Zehfuss et al., 2001). Table 2 summarizes sample information, ^{10}Be concentrations, and calculated exposure ages for both erosion rate scenarios. Use of a nonconstant production rate for these samples yields a <5% (or <1 k.y.) difference in the age calculations.

[1]GSA Data Repository item 2013227, Tabulated $^{40}Ar/^{39}Ar$ results for step heating experiments (Table DR1) and plotted ^{10}Be exposure age versus boulder height (Figure DR1), is available at http://www.geosociety.org/pubs/ft2013.htm or by request to editing@geosociety.org.

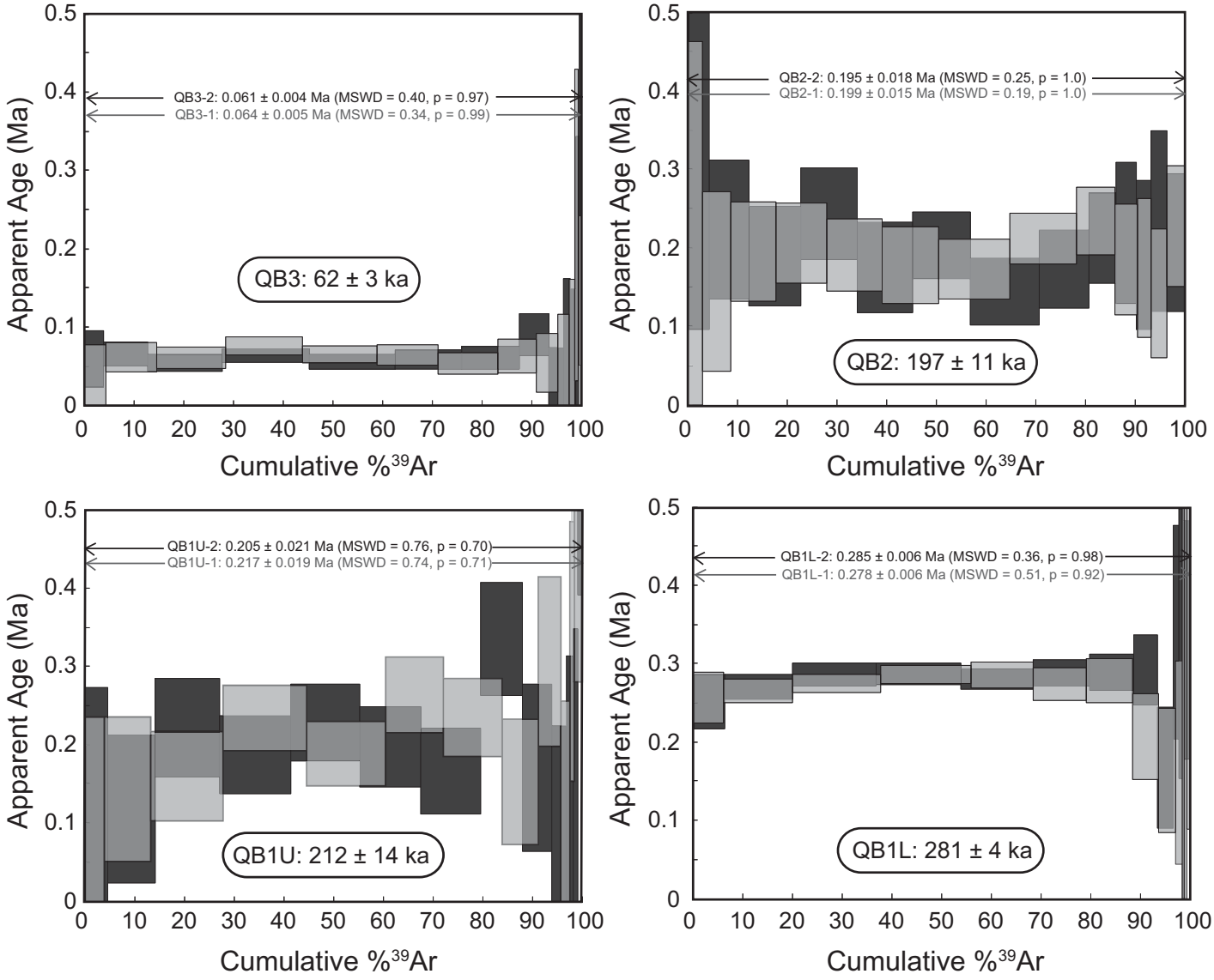

Figure 7. The results of $^{40}Ar/^{39}Ar$ step-heating experiments for the Little Lake basalt flows. Sample locations and geologic unit names are presented in Figure 2. Data for each analysis are presented in Table 1. MSWD—mean square of weighted deviates.

Measured surface exposure ages assuming no boulder erosion vary between ca. 55 and 85 ka, with eight of eleven total ages falling within the range of 60–70 ka (Table 2). Incorporation of in situ boulder erosion rates of 0.2 cm/k.y. yields notably older ages (ca. 61–100 ka; Table 2), although these ages significantly predate the measured eruptive age for the underlying Qb3 basalt (62 ± 3 ka; Table 1). Given the position of the Qt1 and Qt2 boulders on a strath surface eroded into this flow (Fig. 3), incorporation of boulder erosion rates upward of 0.2 cm/k.y. would require a significant component of inherited (i.e., predepositional) ^{10}Be in the measured concentrations. As discussed in the following sections, several arguments point to the absence of substantial cosmogenic inheritance for the Little Lake boulders, thus implying relatively slow or insignificant postdepositional erosion of the sampled boulder tops.

Similarly, the relative height of the sampled boulders above their respective terraces (Table 2) enables evaluation of possible surface lowering or the effects of progressive boulder exhumation on the measured ^{10}Be concentrations. Gradual surface lowering should lead to a positive correlation between measured exposure ages and boulder height (cf. Behr et al., 2010; Rood et al., 2011). No such correlation exists for the Little Lake boulders (Fig. DR1), implying either that surface lowering does not affect the measured age distribution, or that significant exhumation (if present) occurred over a relatively short period of time. In the latter scenario, the measured concentrations would then reflect a significant (and similar) inherited nuclide concentration and the accumulated cosmogenic ^{10}Be subsequent to surface erosion.

The presence or absence of a significant inherited ^{10}Be concentration should be detectable through examination of the total distribution of measured exposure ages. Since large boulders are self-shielding (Behr et al., 2010), the distribution of cosmogenic radionuclides should exhibit substantial variability around (and underneath) the boulder surface. Boulders reworked from an upstream deposit, hillslope, or catchment should produce significant scatter

TABLE 2. ^{10}Be CONCENTRATIONS AND EXPOSURE AGES FOR LITTLE LAKE OUTWASH BOULDERS

Sample name	CAMS ID	Latitude (°)	Longitude (°)	Elevation (m)	Thickness (cm)	Boulder height (m)	Shielding correction*	[^{10}Be] (10^3 atoms g^{-1})†	Exposure age (ka)§ Zero erosion	0.2 cm/k.y. erosion
LL-QT2-01	BE31882	35.9241	–117.9059	902	1.5	1.7	0.994	510.6 ± 9.8	62.1 ± 1.2	69.6 ± 1.5
LL-QT2-02	BE31883	35.9237	–117.9065	900	3.0	1.0	0.994	688.0 ± 13.1	85.4 ± 1.7	100.4 ± 2.3
LL-QT2-03	BE31884	35.9237	–117.9069	905	0.4	1.0	0.994	460.5 ± 13.5	55.3 ± 1.6	61.1 ± 2.0
LL-QT2-04	BE31885	35.9239	–117.9067	904	1.0	1.3	0.994	551.1 ± 11.1	66.8 ± 1.4	75.5 ± 1.8
LL-QT1-01	BE31886	35.9246	–117.9054	908	1.0	1.6	0.994	500.5 ± 13.7	60.3 ± 1.7	67.3 ± 2.1
LL-QT1-02	BE31887	35.9238	–117.9047	900	1.5	0.9	0.994	493.4 ± 9.6	60.1 ± 1.2	67.0 ± 1.5
LL-QT1-03	BE31888	35.9233	–117.9040	902	2.0	1.6	0.994	549.1 ± 14.4	67.2 ± 1.8	76.0 ± 2.3
LL-QT1-04	BE31889	35.9232	–117.9036	905	0.8	1.2	0.994	534.3 ± 13.4	64.5 ± 1.6	72.6 ± 2.1
LL-QT1-05	BE31890	35.9211	–117.9020	900	3.0	1.1	0.987	585.0 ± 11.2	72.9 ± 1.4	83.4 ± 1.9
LL-QT1-06	BE31891	35.9247	–117.9056	908	3.5	1.8	0.994	537.5 ± 10.5	66.2 ± 1.3	74.8 ± 1.7
LL-QT1-07	BE31892	35.9206	–117.9055	896	5.0	0.9	0.994	512.8 ± 9.7	64.5 ± 1.2	72.6 ± 1.6

*Ratio of the production rate at the shielded site to that for a 2π surface at the same location calculated using the CRONUS-Earth Geometric Shielding Calculator version 1.1.

†Calculated using 07KNSTD ^{10}Be measurement standard and calibration with a reported ^{10}Be/^{9}Be ratio of 2.85×10^{-12} (Nishiizumi et al., 2007). Sample ^{10}Be concentrations are corrected for process backgrounds $36.7 \pm 11.1 \times 10^3$ ^{10}Be atoms (0.9%–2.9% of the total ^{10}Be atoms in each of the samples) measured as the average and standard deviation of multiple process blanks. Boron corrections were all less than 0.1%

§Model exposure ages for two boulder erosion rate scenarios (0 and 0.2 cm/k.y.), assuming no inheritance, sample densities of 2.7 g/cm^3, and standard atmosphere calculated using the CRONUS-Earth ^{10}Be-^{26}Al exposure age calculator (Balco et al., 2008) version 2.2 (constants version 2.2.1), using a constant production rate model and scaling scheme for spallation of Lal (1991) and Stone (2000). This version of the CRONUS calculator uses a reference spallogenic ^{10}Be production rate of 4.49 ± 0.39 atoms g^{-1} yr^{-1} (±1σ, sea-level, high-latitude) and muonogenic production after Heisinger et al. (2002a, 2002b). The quoted uncertainty is the 1σ internal error, which reflects accelerator mass spectrometry measurement uncertainty only.

in measured cosmogenic concentrations, given the unlikelihood that an individual clast would come to rest in its initial orientation prior to erosion. A strong cluster or central tendency in a measured exposure age distribution for a number of large boulders argues strongly against the presence of significant inherited cosmogenic radionuclides.

Figure 8 shows individual sample ages and uncertainties (assuming zero boulder erosion) plotted as Gaussian curves, in addition to the composite normal kernel density for all calculated ages. Despite some spread in this distribution from three outlying ages, the composite curve reveals a strong peak from clustered exposure ages between ca. 60 and 70 ka. Much of the total spread comes from two outlying ages from the four samples collected and processed for the younger Qt2 surface. This spread can be attributed to some inherited ^{10}Be for the older sample LL-QT2–02 and postdepositional modification of the younger sample LL-QT2–03. That said, the strong cluster of ages evident from the composite curve between ca. 60 and 70 ka (Fig. 8) argues strongly against a substantial inherited radionuclide component for non-outlying ages.

The eight samples that contribute significantly to this peak provide a mean age of 64.0 ± 5.6 ka (2 standard deviation [SD]) (Fig. 8). Interestingly, the peak age includes samples from both the Qt1 and Qt2 surfaces, which are indistinguishable in the total age spectrum. The three youngest of these ages contribute to a smaller, subpeak in the total distribution, but they also reflect samples from both terrace levels. This overlap suggests that formation of the Qt1 and Qt2 terraces occurred over a short period of time, beyond our ability to resolve distinct ages for each surface from the 11 total samples.

Figure 8. Total results of ^{10}Be exposure dates for surface boulders preserved on the Little Lake terraces. Individual ages are represented using the normal distribution defined by the internal uncertainty for each sample, and apparent peak ages are assessed by calculating the normal kernel density estimate for the total population. Sample information is presented in Table 2.

In summary, the measured distribution of ^{10}Be exposure ages for the Qt1 and Qt2 surfaces in Little Lake narrows does not appear to be substantially affected by postdepositional boulder modification, widespread surface lowering, or substantial inheritance. The stratigraphic position of these boulders above the basalt of Red Hill (Qb3) limits deposition to sometime after 62 ± 3 ka (Table 1). Significant postdepositional erosion of these boulders thus would require a substantial inherited nuclide component—a result incompatible with both the relatively tight cluster of ages between ca. 60 and 70 ka (Fig. 8) and the size of these boulders (≥0.9 m; Table 2). Boulder height does not scale with exposure age, suggesting that any surface lowering (if present) resulted in more than 0.8 m of erosion of both the Qt1 and Qt2 surfaces over a short period of time. This scenario would also require significant inherited radionuclide concentrations, however, that are not inherent in the total age distribution. As such, we favor the simplest interpretation that the sampled boulder tops represent relatively intact portions of largely uneroded clasts, and that the measured exposure ages are not affected by extensive surface erosion or inherited ^{10}Be. Despite our inability to resolve age differences between the Qt1 and Qt2 surfaces, the average exposure age for boulders contributing to the composite peak (64 ± 5.6 ka, 2 SD) provides a relatively tight constraint on the terrace riser separating the upper and lower terrace treads (Fig. 4B).

FAULT-SLIP RATES

Combined geochronologic constraints and offset measurements along the Little Lake fault provide a record of fault-slip rate over the

interval spanning ~10^4–10^5 yr. Slip-rate calculations utilized a Monte Carlo simulation that draws from continuous probability distribution functions (pdf) for both displacement and landform age to generate histograms of slip rate (cf. Thompson et al., 2002). This method presents the distinct advantage of tailoring either discrete or continuous pdfs for offset and age based on any individual set of observations or measurements. Reported slip rates and uncertainties then reflect the mode or peak of the output distribution and the associated 95% confidence intervals after 100,000 trials.

For lateral offsets measured from the Qt1-Qt2 terrace riser (Fig. 5), we used a boxcar or uniform pdf encompassing the total distance range of riser or slope midpoints on either side of the fault. This distribution represents a conservative approach, given that we avoided choosing a subjective, preferred value of slip common for estimates based on two-dimensional image restoration. Similarly, we used a uniform pdf to characterize dextral offset of the eastern wall of Little Lake narrows, bounded by the minimum and maximum displacement estimates from our geometric reconstruction (Fig. 6). This approach is considerably less certain than offset of the Qt1-Qt2 terrace riser. We argue that wherever possible, offset reconstructions should rely on the actual geomorphic and topographic variability (readily observable with lidar) of displaced landforms along strike-slip faults (cf. Frankel and Dolan, 2007).

Considerable discussion surrounds the application of surface ages in fault-slip rate calculations measured from the intervening terrace riser (Cowgill, 2007). This debate centers on whether ages for the upper or lower terrace surfaces better constrain the timing of riser formation and thus fault displacement. Similar ages for the upper Qt1 and lower Qt2 surfaces (Fig. 8), however, suggest that terraces in Little Lake narrows formed over a relatively short period of time (≤~10 k.y.). As such, we utilize the mean age (64.0 ± 5.6 ka, 2 SD) for non-outlying samples present on the upper and lower surfaces bounding the Qt1-Qt2 riser (Fig. 5). By treating this peak age as normally distributed and assigning uniform probability to displacements between 30 and 42 m and 34 and 49 m for the western and eastern margins of the Qt1 terrace, respectively, we calculate dextral slip rates of 0.6 ± 0.2 mm/yr at 95% confidence (Fig. 9).

Similarly, we lack direct age control on the offset eastern margin of Little Lake narrows. New $^{40}Ar/^{39}Ar$ dates, however, indicate that channel erosion occurred sometime after eruption of the upper Qb1 flow at 212 ± 14 ka, and before Qb2 basalt inundated the Owens River channel at 197 ± 11 ka (Fig. 7). These two ages overlap within error and provide a relatively tight bracketing age for the offset cliff. Accordingly, we utilized the composite pdf of both $^{40}Ar/^{39}Ar$ ages in order to encompass uncertainty in the timing of canyon incision. In combination with the minimum and maximum displacement estimates from our geometric reconstruction (~140–250 m; Fig. 6), this age suggests between 0.7 and 1.3 mm/yr of dextral slip at 95% confidence (Fig. 9).

DISCUSSION

Geomorphic Implications for the Pleistocene Owens River

Newly revised geochronology within Little Lake narrows sheds light on the timing and processes governing geomorphic and volcanic interactions in the Pleistocene Owens River. In particular, results from $^{40}Ar/^{39}Ar$ dating of the Little Lake basalts coupled with ^{10}Be exposure dating of terrace surfaces demonstrate that volcanic eruptions from the Coso Range closely coincided with the timing of incision through Little Lake narrows. As originally recognized by Duffield and Smith (1978a), the earliest cycle of canyon incision through Little Lake occurred after eruption of the Qb1 flow, as the Owens River was subsequently diverted from its former eastern course through the western Coso Range (Fig. 2). Our revised chronology constrains this incision to sometime after 212 ± 14 ka and before the oldest intracanyon flow, Qb2, occupied the channel at 197 ± 11 ka (Fig. 7). Base-level fall associated with this downcutting event drove incision into alluvial fans flanking the eastern Sierra margin (Fig. 2), isolating the upper fan surfaces from subsequent

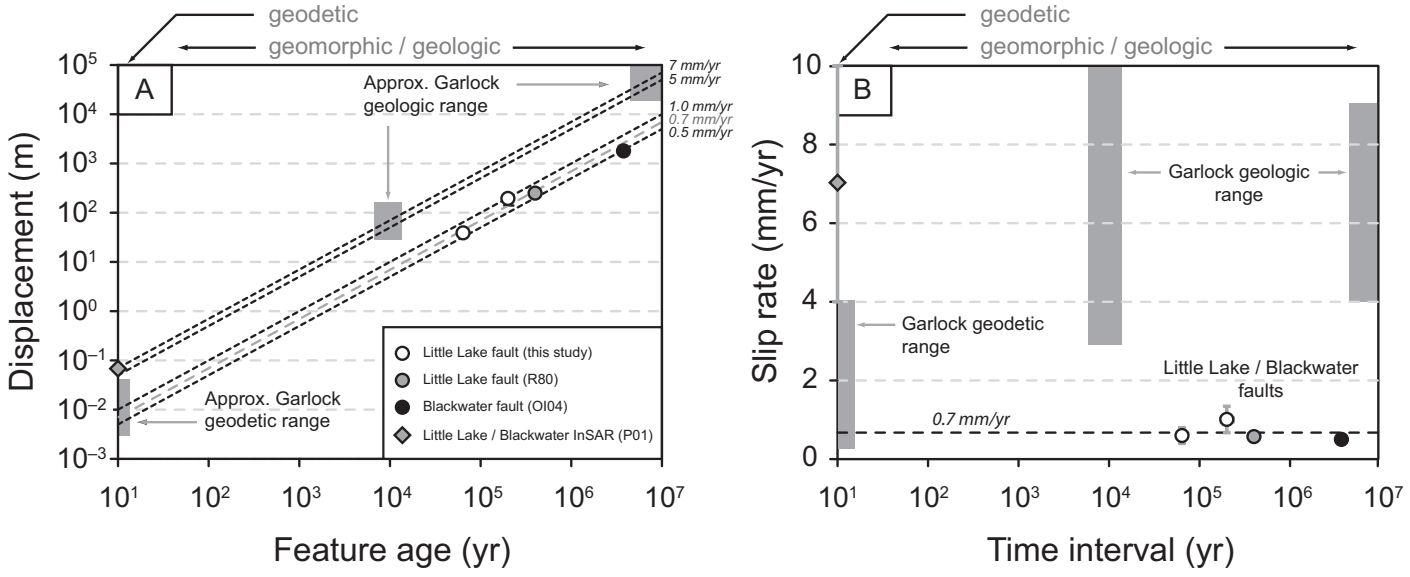

Figure 9. (A) Compiled dextral displacements and (B) corresponding fault-slip rates as a function of age for the Little Lake, Blackwater, and Garlock faults. Linear regressions in A indicate constant slip rates through time. Geologic slip rate estimates in B are for time intervals since the respective age measurements. Geodetic measurements represent interseismic deformation measured from interferometric synthetic aperture radar (InSAR) and global positioning system (GPS). Source abbreviations are as follows: R80—Roquemore (1980); OI04—Oskin and Iriondo (2004); P01—Peltzer et al. (2001). See Ganev et al. (2012) for a summary of Garlock fault measurements.

deposition. The isolated remnants of these older alluvial fans remain perched above the incised canyon floor today (Fig. 4A). Although the exact cause of this initial diversion is unknown (Duffield and Smith, 1978a), overlap between the two bracketing canyon ages suggests that incision closely followed eruption of the upper Qb1 flow.

The prominent erosional escarpment east of Little Lake indicates that widespread channel incision also followed eruption of the intermediate Qb2 flow (Fig. 2). This channel may have followed a former course along the western margin of Rose Valley, although younger alluvial fans and the basalt of Red Hill obscure its original path (Fig. 3). Several prominent fluvial trimlines that cut into older alluvial-fan deposits mark the northwestern edge of this channel (Fig. 3). Whether these features represent erosion following eruption of Qb2 or the younger Qb3 flow remains unclear. Nevertheless, incision following either the upper Qb1 or intracanyon Qb2 flows coincides generally with the onset of marine isotope stage (MIS) 6, a time when high shorelines of Owens Lake to the north indicate overflowing conditions (Jayko and Bacon, 2008). Erosional trimlines at the southern end of Rose Valley thus serve as possible downstream geomorphic evidence of this former lake highstand. The sill for the MIS 6 Owens Lake has either been removed by erosion or displaced by faulting, and it remains unclear whether the lake stretched as far south as Rose Valley (Jayko and Bacon, 2008).

A third cycle of channel erosion is well constrained by $^{40}Ar/^{39}Ar$ dating of the Red Hill basalt (Qb3) at 62 ± 3 ka (Fig. 7) and subsequent deposition of the Qt1-Qt2 boulders at 64 ± 5.6 ka (Fig. 8). This event resulted in widespread erosion of the canyon floor, evidenced by the prominent strath cut into the Qb3 flow at a lower elevation than intact flow remnants flanking the western channel edge (Fig. 3). These age relations suggest a causal linkage between basaltic eruption into the Owens River channel and subsequent channel erosion. We speculate that strath cutting and deposition of meter-scale boulders to form the Qt1-Qt2 terrace surfaces (Fig. 4) could be linked to outburst flooding following breach of an upstream lava dam created by the Red Hill basalt. In this scenario, similar ages for boulders on both surfaces result from initial deposition of the Qt1 terrace followed by channelization and incision of this surface during waning flow to create the Qt2 surface as a cut terrace. Later burial of the upstream channel by younger alluvial fans, however, obscures the position of the hypothesized lava dam (Fig. 3). Nevertheless, our results indicate overflowing conditions in the Owens River drainage at ca. 64 ka that were sufficient to rapidly pond an upstream shallow lake through Little Lake narrows. Subsequent pluvial drainage from the upstream Owens Lake during and after the Last Glacial Maximum (LGM) (Bacon et al., 2006) localized the most recent course of the Owens River east of Red Hill and across Fossil Falls (Fig. 2). Despite dramatic evidence for fluvial erosion over this cascade, this outflow may have remained largely confined within the inset river channel holding the modern Little Lake (Fig. 3) and was likely significantly smaller than the previous erosional events.

Geomorphic Uncertainties

Evaluation of new slip rate estimates requires discussion of additional uncertainties and assumptions not captured by our geochronologic or offset measurements and their error estimates. In particular, we consider alternative geomorphic interpretations to explain the ages and overlap for boulders on the Qt1-Qt2 surfaces (Fig. 8). Given the variety of geomorphic and stratigraphic evidence indicating overflowing conditions in Owens Lake throughout the LGM (cf. Bacon et al., 2006), it is somewhat surprising that boulders (and surfaces) with a mean exposure age of ca. 64 ka survived only several meters above the floor of the river channel. Bacon et al. (2006) documented at least 15 m of sill lowering over this period, with the last outflow ceasing by ca. 15,300 cal yr B.P. This estimate overlaps with the timing of fluvial scour at Fossil Falls between ca. 16 and 17 ka, based on ^{3}He exposure ages on the Red Hill basalt (Cerling, 1990). In light of this evidence for systemwide channel erosion, the lack of young exposure ages could suggest that LGM and younger drainage was diverted around the Qt1 and Qt2 surfaces. This scenario would imply that significant outflow during sill erosion and scour of Fossil Falls remained confined to the inset channel immediately east of these terraces (Figs. 3 and 4) or was routed through a now-buried channel beneath young alluvial-fan deposits immediately to the west (Fig. 3). Similar exposure ages for the Qt1 and Qt2 boulders in this scenario reflect original deposition of the Qt1 boulders followed closely by incision and formation of the inset Qt2 surface.

Alternatively, formation of the Qt2 surface as a cut terrace into Qt1 terrace fill may reflect LGM and younger erosion by the Pleistocene Owens River. In this scenario, the Qt2 surface would have formed long after deposition of the Qt1 boulders at ca. 64 ka by reworking and incision into the ~5-m-thick terrace cover. This scenario matches the observation of a patchy Qt2 terrace cover above the underlying basalt strath. If true, by sampling only the largest intact boulders on the Qt2 terrace, we may have systematically biased our ages to clasts not washed away during erosional reworking of the Qt1 and Qt2 surfaces and formation of the intervening riser. Such a scenario would imply that this feature began accumulating displacement along the Little Lake fault over a much younger interval. If true, our estimated slip rates of 0.6 ± 0.2 mm/yr represent absolute minimum bounds on slip rates that could reach as high as ~1–3 mm/yr.

The observed distribution of ^{10}Be exposure ages on both the Qt1 and Qt2 surfaces (Fig. 8), however, argues against significant postdepositional surface lowering or rapid exhumation. The strong age peak at ca. 64 ka from eight of eleven sampled boulders implies that these clasts do not reflect a substantial inherited nuclide component, given that they are large enough to be self-shielding (Behr et al., 2010). Rapid exhumation of these boulders during LGM or younger Owens River drainage should have led to significant scatter beyond that observed in the calculated exposure ages (Fig. 8). Similarly, exposure ages do not scale with boulder height (Fig. DR1 [see footnote 1]), arguing against gradual exhumation or surface lowering since deposition.

Second, the former river channel connecting Fossil Falls through the Little Lake narrows is inset below the Qt1 and Qt2 terraces up to ~5 m above the modern lake level (Fig. 3). This channel and its margins are continuous through the narrows and connect drainage through the active wash downstream to Indian Wells Valley (Fig. 2). As discussed in the previous section, this inset channel is superimposed on surfaces and deposits likely formed during a larger, canyonwide erosion event at ca. 64 ka.

Several observations, however, point to some degree of channel overtopping and reworking of the inset Qt2 terrace surface and its comparatively patchy boulder cover. First, the elevation of this surface at its northern end is within a few meters of the floor of the active wash (Fig. 4B). As such, the Qt2 surface is vulnerable to drainage through Little Lake wash in the absence of a concealed channel now buried by young alluvial fans to the west. Exposure ages for the Qt2 boulders also exhibit significantly more scatter than Qt1 (Fig. 8), with two of four samples showing evidence of bias due to either erosion or inheritance. The presence of two non-outlying ages, however, implies that LGM and younger drainage did not result in complete stripping of this surface. Given that the Qt1-Qt2 terrace riser consists of similarly sized boulders, we suggest that postdepositional reworking was insufficient to completely refresh this landform. As such, slip rates calculated using the composite

peak age of ca. 64 ka (0.6 ± 0.2 mm/yr) represent average values over this interval rather than absolute minimum constraints.

Implications for Eastern California Shear Zone Active Tectonics

The combined results of surficial mapping, surveying, and surface dating in Little Lake narrows suggest steady, modest rates of dextral slip averaging at least ~0.6–1.3 mm/yr over the past ~200 k.y. (Fig. 9). This rate is similar to previous estimates for the Little Lake fault (0.6 mm/yr) based on K-Ar dating and geometric consideration of the offset Qb1 basalt (Roquemore, 1980). Slip rates on the Little Lake fault also mirror Quaternary-integrated slip on the Blackwater fault in the northern Mojave Desert (Fig. 1) of ~0.5 mm/yr (Oskin and Iriondo, 2004). Our results confirm that slip on the Little Lake fault is outpaced by several-fold-faster rates on the conjugate Garlock structure (Fig. 9).

Similarity between slip rate measurements over the past ~64 k.y. and 200 k.y. restricts hypothesized temporal fluctuations in slip on the Little Lake–Blackwater faults to occur over time intervals between ~10^1 and 10^3 yr (Fig. 9). Neither fault has produced a large, historical surface rupture, although numerous Holocene earthquakes are documented along the correspondingly faster-slipping Garlock fault (Dawson et al., 2003). As such, our results leave open the possibility that anomalously fast interseismic velocities observed from geodetic data spanning the Little Lake fault (Hearn and Humphreys, 1998; Gan et al., 2000; McClusky et al., 2001; Peltzer et al., 2001) are sustained over multiple earthquake cycles.

Updated interferometric synthetic aperture radar (InSAR) time-series data spanning the Little Lake–Blackwater fault, however, suggest a marked decrease in this interseismic velocity over the past decade (Peltzer et al., 2010). These authors attribute earlier, rapid fault loading (consistent with a modeled slip rate of 7 ± 3 mm/yr during 1992–2000; Peltzer et al., 2001) to a pulse of transiently increased strain following the 1992 Landers earthquake (Fig. 1). If true, this result indicates that elevated loading along the Little Lake and Blackwater faults may be truly transient over comparatively short periods of time. Coupled with new geologic evidence for sustained, sub-millimeter-per-year dextral slip on the Little Lake fault (Fig. 9), such transients need not manifest as temporal fluctuations in slip rate over geologic intervals. Although we do not discount earlier hypotheses related to temporal shifts in activity between the conjugate Little Lake–Blackwater and Garlock faults (Peltzer et al., 2001; Dolan et al., 2007), we find no evidence for sustained rate changes over periods between ~10^4 and 10^5 yr.

Nevertheless, the possibility that the 1992 Landers earthquake drove transient shear localized about the Little Lake fault raises a number of intriguing questions about fault interconnectivity and earthquake strain in the Eastern California shear zone. Chief among these is the possibility that transient, interseismic strain may somehow localize along intervening shear zones between earthquake ruptures, perhaps even over regional distances (Bodin and Gomberg, 1994). Such a localized zone of transient postseismic deformation at large distance from the Landers rupture suggests the existence and important role of narrow weak zones below the seismogenic crust not generally considered in postseismic model studies (Pollitz et al., 2000; Fialko, 2004; Freed and Burgmann, 2004). As discussed by Oskin and Iriondo (2004), such temporarily increased fault loading from the Landers and Owens Valley earthquakes (Fig. 1) could thus drive the Blackwater and Little Lake faults closer to failure, thus enhancing the near-term seismic hazard associated with these structures. This work clearly shows the importance of multitemporal slip-rate data in detecting areas where interseismic strain exceeds time-averaged geologic slip rates.

CONCLUSIONS

The combined results of new geochronologic and survey measurements yield insights into Pleistocene tectonic, geomorphic, and volcanic interactions in the Little Lake area. A clear result from this work is the impact of nearby basaltic eruptions into the Owens River channel in influencing the pattern and timing of canyon erosion and landform development. Newly revised chronologic constraints from $^{40}Ar/^{39}Ar$ and ^{10}Be dating suggest avulsion of the Owens River channel to its present position between 212 ± 14 and 197 ± 11 ka, and canyonwide erosion and outburst flooding following breach of an upstream lava dam at ca. 64 ka. We recognize at least four episodes of pluvial drainage through the Little Lake channel, the youngest associated with comparatively modest erosion of Fossil Falls following the LGM. Although sufficient discharge to create these flows largely depends on the prevailing climatic conditions, the geomorphic development of this portion of the Pleistocene Owens River strongly reflects the timing and impact of intracanyon volcanic eruptions.

Modest and steady dextral slip along the Little Lake fault averages between ~0.6 and 1.3 mm/yr over these cycles of canyon erosion. Although we lack constraints on this rate over the time scales corresponding to earthquake clusters in the Eastern California shear zone (~10^3 yr; Rockwell et al., 2000; Dawson et al., 2003), we find no evidence for fluctuations in slip that approach the comparatively fast interseismic loading rate observed from early geodetic studies. Instead, rapid interseismic strain along the Little Lake fault appears to be truly transient over short periods, possibly related to the 1992 Landers earthquake rupture (Peltzer et al., 2010). The way in which such localized strain is transmitted over ~100 km across the Garlock fault remains an outstanding research question. Nevertheless, our well-constrained slip rates for the Little Lake fault indicate that such transients may elevate interseismic strain well above the background loading rate, and may temporarily increase the likelihood of fault rupture.

ACKNOWLEDGMENTS

We thank Bruce Ivey and Dan Tolbert at Little Lake Ranch, and Paul Hancock and Anita McProud of Lone Pine, California. We are also grateful for comments and suggestions in the field from the 2011 Pacific Cell of the Friends of the Pleistocene. Helpful reviews by Ken Adams, Mike Oskin, Katherine Kendrick, and the associate editor, Eric Kirby, significantly improved this paper. This research was supported by National Science Foundation Postdoctoral Fellowship Award EAR-0847990 to Amos.

REFERENCES CITED

Amos, C.B., Lutz, A.T., Jayko, A.S., Mahan, S.A., Fisher, G.B., and Unruh, J.R., 2013, Refining the southern extent of the 1872 Owens Valley earthquake rupture through paleoseismic investigations in the Haiwee area, southeastern California: Bulletin of the Seismological Society of America, v. 103, p. 1022–1037, doi:10.1785/0120120024.

Argus, D.F., and Gordon, R.G., 1991, Current Sierra Nevada–North America motion from very long baseline interferometry: Implications for the kinematics of the western United States: Geology, v. 19, p. 1085–1088, doi:10.1130/0091-7613(1991)019<1085:CSNNAM>2.3.CO;2.

Bacon, S.N., Jayko, A.S., and McGeehin, J.P., 2005, Holocene and latest Pleistocene oblique dextral faulting on the southern Inyo Mountains fault, Owens Lake Basin, California: Bulletin of the Seismological Society of America, v. 95, p. 2472–2485, doi:10.1785/0120040228.

Bacon, S.N., Burke, R.M., Pezzopane, S.K., and Jayko, A.S., 2006, Last Glacial Maximum and Holocene lake levels of Owens Lake, eastern California, USA: Quaternary Science Reviews, v. 25, p. 1264–1282, doi:10.1016/j.quascirev.2005.10.014.

Balco, G., Stone, J., Lifton, N., and Dunai, T., 2008, A simple, internally consistent, and easily accessible means of calculating surface exposure ages and erosion rates from Be-10 and Al-26 measurements: Quaternary Geochronology, v. 3, p. 174–195, doi:10.1016/j.quageo.2007.12.001.

Behr, W.M., Rood, D.H., Fletcher, K.E., Guzman, N., Finkel, R., Hanks, T.C., Hudnut, K.W., Kendrick, K.J., Platt, J.P., Sharp, W.D., Weldon, R.J., and Yule, J.D., 2010, Uncertainties in slip-rate estimates for the Mission Creek strand of the southern San Andreas fault at Biskra Palms Oasis, southern California: Geological Society of America Bulletin, v. 122, p. 1360–1377, doi:10.1130/B30020.1.

Bennett, R.A., Wernicke, B.P., Niemi, N.A., Friedrich, A.M., and Davis, J.L., 2003, Contemporary strain rates in the northern Basin and Range Province from GPS data: Tectonics, v. 22, 1008, doi:10.1029/2001TC001355.

Blackwelder, E., 1933, Lake Manly, an extinct lake of Death Valley: Geographical Review, v. 23, p. 464–471, doi:10.2307/209632.

Bodin, P., and Gomberg, J., 1994, Triggered seismicity and deformation between the Landers, California, and Little-Skull-Mountain, Nevada, earthquakes: Bulletin of the Seismological Society of America, v. 84, p. 835–843.

Brossy, C.C., Kelson, K.I., Amos, C.B., Baldwin, J.N., Kozlowicz, B., Simpson, D., Ticci, M.G., Lutz, A.T., Kozaci, O., Streig, A., Turner, R., and Rose, R., 2012, Map of the late Quaternary active Kern Canyon and Breckenridge faults, southern Sierra Nevada, California: Geosphere, v. 8, p. 581–591, doi:10.1130/GES00663.1.

Cerling, T.E., 1990, Dating geomorphologic surfaces using cosmogenic He-3: Quaternary Research, v. 33, p. 148–156, doi:10.1016/0033-5894(90)90015-D.

Chuang, R.Y., and Johnson, K.M., 2011, Reconciling geologic and geodetic model fault slip-rate discrepancies in Southern California: Consideration of nonsteady mantle flow and lower crustal fault creep: Geology, v. 39, p. 627–630, doi:10.1130/G32120.1.

Cowgill, E., 2007, Impact of riser reconstructions on estimation of secular variation in rates of strike-slip faulting: Revisiting the Cherchen River site along the Altyn Tagh fault, NW China: Earth and Planetary Science Letters, v. 254, p. 239–255, doi:10.1016/j.epsl.2006.09.015.

Dawson, T.E., McGill, S.F., and Rockwell, T.K., 2003, Irregular recurrence of paleoearthquakes along the central Garlock fault near El Paso Peaks, California: Journal of Geophysical Research–Solid Earth, v. 108, 2356, doi:10.1029/2001JB001744.

DeMets, C., Gordon, R.G., and Argus, D.F., 2010, Geologically current plate motions: Geophysical Journal International, v. 181, p. 1–80, doi:10.1111/j.1365-246X.2009.04491.x.

Ditchburn, R.G., and Whitehead, N.E., 1994, The separation of ^{10}Be from silicates: Proceedings of the 3rd Workshop of the South Pacific Environmental Radioactivity Association: Canberra, Australia, South Pacific Environmental Radioactivity Association, p. 4–7.

Dixon, T.H., Miller, M., Farina, F., Wang, H., and Johnson, D., 2000, Present-day motion of the Sierra Nevada block and some tectonic implications for the Basin and Range Province, North American Cordillera: Tectonics, v. 19, p. 1–24, doi:10.1029/1998TC001088.

Dixon, T.H., Norabuena, E., and Hotaling, L., 2003, Paleoseismology and global positioning system: Earthquake-cycle effects and geodetic versus geologic fault slip rates in the Eastern California shear zone: Geology, v. 31, p. 55–58, doi:10.1130/0091-7613(2003)031<0055:PAGPSE>2.0.CO;2.

Dokka, R.K., and Travis, C.J., 1990, Late Cenozoic strike-slip faulting in the Mojave Desert, California: Tectonics, v. 9, p. 311–340, doi:10.1029/TC009i002p00311.

Dolan, J.F., Bowman, D.D., and Sammis, C.G., 2007, Long-range and long-term fault interactions in Southern California: Geology, v. 35, p. 855–858, doi:10.1130/G23789A.1.

Duffield, W.A., and Bacon, C.R., 1981, Geologic Map of the Coco Volcanic Field and Adjacent Areas, Inyo County, California: U.S. Geological Survey Miscellaneous Investigations Series, I-1200, scale 1:50,000.

Duffield, W.A., and Smith, G.I., 1978a, Pleistocene history of volcanism and Owens River near Little Lake, California: Journal of Research of the U.S. Geological Survey, v. 6, no. 3, p. 395–408.

Duffield, W.A., and Smith, G.I., 1978b, Pleistocene river erosion and intracanyon lava flows near Little Lake, Inyo County, California: California Geology, v. 31, p. 81–89.

Duffield, W.A., Bacon, C.R., and Dalrymple, G.B., 1980, Late Cenozoic volcanism, geochronology, and structure of the Coso Range, Inyo County, California: Journal of Geophysical Research, v. 85, p. 2381–2404, doi:10.1029/JB085iB05p02381.

Fialko, Y., 2004, Evidence of fluid-filled upper crust from observations of postseismic deformation due to the 1992 M(w)7.3 Landers earthquake: Journal of Geophysical Research–Solid Earth, v. 109, B08401, doi:10.1029/2004JB002985.

Fisher, G.B., Amos, C.B., Bookhagen, B., Burbank, D.W., and Godard, V., 2012, Channel widths, landslides, faults, and beyond: The new world order of high-spatial resolution Google Earth imagery in the study of earth surface processes, *in* Whitmeyer, S.J., De Paor, D.G., Bailey, J., and Ornduff, T., eds., Google Earth and Virtual Visualizations in Geoscience Education and Research: Geological Society of America Special Paper 492, p. 1–22, doi:10.1130/2012.2492(1101).

Frankel, K.L., and Dolan, J.F., 2007, Characterizing arid region alluvial fan surface roughness with airborne laser swath mapping digital topographic data: Journal of Geophysical Research, v. 112, F02025, doi:10.1029/2006JF000644.

Frankel, K.L., Brantley, K.S., Dolan, J.F., Finkel, R.C., Klinger, R.E., Knott, J.R., Machette, M.N., Owen, L.A., Phillips, F.M., Slate, J.L., and Wernicke, B.P., 2007a, Cosmogenic Be-10 and Cl-36 geochronology of offset alluvial fans along the northern Death Valley fault zone: Implications for transient strain in the Eastern California shear zone: Journal of Geophysical Research–Solid Earth, v. 112, B06407, doi:10.1029/2006JB004350.

Frankel, K.L., Dolan, J.F., Finkel, R.C., Owen, L.A., and Hoeft, J.S., 2007b, Spatial variations in slip rate along the Death Valley–Fish Lake Valley fault system determined from LiDAR topographic data and cosmogenic Be-10 geochronology: Geophysical Research Letters, v. 34, L18303, doi:10.1029/2007GL030549.

Frankel, K.L., Dolan, J.F., Owen, L.A., Ganev, P., and Finkel, R.C., 2011, Spatial and temporal constancy of seismic strain release along an evolving segment of the Pacific–North America plate boundary: Earth and Planetary Science Letters, v. 304, p. 565–576, doi:10.1016/j.epsl.2011.02.034.

Freed, A.M., and Burgmann, R., 2004, Evidence of power-law flow in the Mojave Desert mantle: Nature, v. 430, p. 548–551, doi:10.1038/nature02784.

Friedrich, A.M., Wernicke, B.P., Niemi, N.A., Bennett, R.A., and Davis, J.L., 2003, Comparison of geodetic and geologic data from the Wasatch region, Utah, and implications for the spectral character of Earth deformation at periods of 10 to 10 million years: Journal of Geophysical Research–Solid Earth, v. 108, 2199, doi:10.1029/2001JB000682.

Gale, H.S., 1914, Notes on the Quaternary lakes of the Great Basin, with special reference to the deposition of potash and other salines: U.S. Geological Survey Bulletin 540, p. 399–406.

Gan, W.J., Svarc, J.L., Savage, J.C., and Prescott, W.H., 2000, Strain accumulation across the Eastern California shear zone at latitude 36°30′N: Journal of Geophysical Research–Solid Earth, v. 105, p. 16,229–16,236, doi:10.1029/2000JB900105.

Ganev, P.N., Dolan, J.F., McGill, S.F., and Frankel, K.L., 2012, Constancy of geologic slip rate along the central Garlock fault: Implications for strain accumulation and release in southern California: Geophysical Journal International, v. 190, no. 2, p. 745–706, doi:10.1111/j.1365-246X.2012.05494.x.

Gold, P.O., Cowgill, E., Kreylos, O., and Gold, R.D., 2012, A terrestrial LiDAR-based workflow for determining three-dimensional slip vectors and associated uncertainties: Geosphere, v. 8, p. 431–442, doi:10.1130/GES00714.1.

Gold, R.D., Cowgill, E., Arrowsmith, J.R., Gosse, J., Chen, X., and Wang, X.-F., 2009, Riser diachroneity, lateral erosion, and uncertainty in rates of strike-slip faulting: A case study from Tuzidun along the Altyn Tagh fault, NW China: Journal of Geophysical Research–Solid Earth, v. 114, no. B4, B04401, doi:10.1029/2008JB005913.

Gold, R.D., Cowgill, E., Arrowsmith, J.R., Chen, X., Sharp, W.D., Cooper, K.M., and Wang, X.-F., 2011, Faulted terrace risers place new constraints on the late Quaternary slip rate for the central Altyn Tagh fault, northwest Tibet: Geological Society of America Bulletin, v. 123, p. 958–978, doi:10.1130/B30207.1.

Hauksson, E., Hutton, K., Kanamori, H., Jones, L., Mori, J., Hough, S., and Roquemore, G., 1995, Preliminary report on the 1995 Ridgecrest earthquake sequence in eastern California: Seismological Research Letters, v. 66, p. 54–60, doi:10.1785/gssrl.66.6.54.

Hearn, E.H., and Humphreys, E.D., 1998, Kinematics of the southern Walker Lane belt and motion of the Sierra Nevada block, California: Journal of Geophysical Research–Solid Earth, v. 103, p. 27,033–27,049, doi:10.1029/98JB01390.

Heisinger, B., Lal, D., Jull, A.J.T., Kubik, P.W., Ivy-Ochs, S., Neu- maier, S., Knie, K., Lazarev, V., and Nolte, E., 2002a, Pro- duction of selected cosmogenic radionuclides by muons: 1. Fast muons: Earth and Planetary Science Letters, v. 200, p. 345–355, doi:10.1016/S0012-821X(02)00640-4.

Heisinger, B., Lal, D., Jull, A.J.T., Kubik, P.W., Ivy-Ochs, S., Neumaier, S., Knie, K., Lazarev, V., and Nolte, E., 2002b, Production of selected cosmogenic radionuclides by muons: 2. Capture of negative muons: Earth and Planetary Science Letters, v. 200, p. 357–369, doi:10.1016/S0012-821X(02)00641-6.

Jannik, N.O., Phillips, F.M., Smith, G.I., and Elmore, D., 1991, A Cl-36 chronology of lacustrine sedimentation in the Pleistocene Owens River system: Geological Society of America Bulletin, v. 103, p. 1146–1159, doi:10.1130/0016-7606(1991)103<1146:ACCOLS>2.3.CO;2.

Jayko, A.S., and Bacon, S.N., 2008, Late Quaternary MIS 6–8 shoreline features of pluvial Owens Lake, Owens Valley, eastern California, *in* Reheis, M.C., Hershler, R., and Miller, D.M., eds., Late Cenozoic Drainage History of the Southwestern Great Basin and Lower Colorado River Region: Geologic and Biotic Perspectives: Geological Society of America Special Paper 439, p. 185–206, doi:10.1130/2008.2439(08).

Kirby, E., Burbank, D.W., Reheis, M., and Phillips, F., 2006, Temporal variations in slip rate of the White Mountain fault zone, eastern California: Earth and Planetary Science Letters, v. 248, p. 168–185, doi:10.1016/j.epsl.2006.05.026.

Kirby, E., Anandakrishnan, S., Phillips, F., and Marrero, S., 2008, Late Pleistocene slip rate along the Owens Valley fault, eastern California: Geophysical Research Letters, v. 35, L01304, doi:10.1029/2007GL031970.

Kohl, C.P., and Nishiizumi, K., 1992, Chemical isolation of quartz for measurement of in-situ–produced cosmogenic nuclides: Geochimica et Cosmochimica Acta, v. 56, p. 3583–3587, doi:10.1016/0016-7037(92)90401-4.

Lal, D., 1991, Cosmic ray labeling of erosion surfaces: In situ nuclide production rates and erosion models: Earth and Planetary Science Letters, v. 104, p. 424–439, doi:10.1016/0012-821X(91)90220-C.

Lanphere, M.A., Dalrymple, G.B., and Smith, R.L., 1975, K-Ar ages of Pleistocene rhyolitic volcanism in Coso Range, California: Geology, v. 3, p. 339–343, doi:10.1130/0091-7613(1975)3<339:KAOPRV>2.0.CO;2.

Lee, J., Spencer, J., and Owen, L., 2001, Holocene slip rates along the Owens Valley fault, California: Implications for the recent evolution of the Eastern California shear zone: Geology, v. 29, p. 819–822, doi:10.1130/0091-7613(2001)029<0819:HSRATO>2.0.CO;2.

McClusky, S.C., Bjornstad, S.C., Hager, B.H., King, R.W., Meade, B.J., Miller, M.M., Monastero, F.C., and Souter, B.J., 2001, Present-day kinematics of the Eastern California shear zone from a geodetically constrained block model: Geophysical Research Letters, v. 28, p. 3369–3372, doi:10.1029/2001GL013091.

McGill, S.F., Wells, S.G., Fortner, S.K., Kuzma, H.A., and McGij, J.D., 2009, Slip rate of the western Garlock fault, at Clark Wash, near Lone Tree Canyon, Mojave Desert, California: Geological Society of America Bulletin, v. 121, p. 536–554, doi:10.1130/B26123.1.

Meade, B.J., and Hager, B.H., 2005, Block models of crustal motion in southern California constrained by GPS measurements: Journal of Geophysical Research–Solid Earth, v. 110, B03403, doi:10.1029/2004JB003209.

Mehringer, P.J., and Sheppard, J.C., 1978, Holocene history of Little Lake, Mojave Desert, California, *in* Davis, E.L., ed., The Ancient Californians: Ranchoalbrean Hunters of the Mojave Lakes Country: Los Angeles, Natural History Museum of Los Angeles County, p. 153–166.

Miller, M.M., Johnson, D.J., Dixon, T.H., and Dokka, R.K., 2001, Refined kinematics of the Eastern California shear zone from GPS observations, 1993–1998: Journal of Geophysical Research–Solid Earth, v. 106, p. 2245–2263, doi:10.1029/2000JB900328.

Monastero, F.C., Katzenstein, A.M., Miller, J.S., Unruh, J.R., Adams, M.C., and Richards-Dinger, K., 2005, The Coso geothermal field: A nascent metamorphic

core complex: Geological Society of America Bulletin, v. 117, p. 1534–1553, doi:10.1130/B25600.1.

Nishiizumi, K., Imamura, M., Caffee, M., Southon, J., Finkel, R., and McAnich, J., 2007, Absolute calibration of ^{10}Be AMS standards: Nuclear Instruments & Methods in Physics Research, Section B, Beam Interactions with Materials and Atoms, v. 258, p. 403–413, doi:10.1016/j.nimb.2007.01.297.

Oldow, J.S., and Singleton, E.S., 2008, Application of terrestrial laser scanning in determining the pattern of late Pleistocene and Holocene fault displacement from the offset of pluvial lake shorelines in the Alvord extensional basin, northern Great Basin, USA: Geosphere, v. 4, p. 536–563, doi:10.1130/GES00101.1.

Oskin, M., and Iriondo, A., 2004, Large-magnitude transient strain accumulation on the Blackwater fault, Eastern California shear zone: Geology, v. 32, p. 313–316, doi:10.1130/G20223.1.

Oskin, M., Perg, L., Blumentritt, D., Mukhopadhyay, S., and Iriondo, A., 2007, Slip rate of the Calico fault: Implications for geologic versus geodetic rate discrepancy in the Eastern California shear zone: Journal of Geophysical Research–Solid Earth, v. 112, no. B3, doi:10.1029/2006JB004451.

Oskin, M., Perg, L., Shelef, E., Strane, M., Gurney, E., Singer, B., and Zhang, X., 2008, Elevated shear zone loading rate during an earthquake cluster in eastern California: Geology, v. 36, p. 507–510, doi:10.1130/G24814A.1.

Pelletier, J.D., DeLong, S.B., Al-Suwaidi, A.H., Cline, M., Lewis, Y., Psillas, J.L., and Yanites, B., 2006, Evolution of the Bonneville shoreline scarp in west-central Utah: Comparison of scarp-analysis methods and implications for the diffusion model of hillslope evolution: Geomorphology, v. 74, p. 257–270, doi:10.1016/j.geomorph.2005.08.008.

Peltzer, G., Crampe, F., Hensley, S., and Rosen, P., 2001, Transient strain accumulation and fault interaction in the Eastern California shear zone: Geology, v. 29, p. 975–978, doi:10.1130/0091-7613(2001)029<0975:TSAAFI>2.0.CO;2.

Peltzer, G., Liu, Z., and Lundgren, P., 2010, Time series analysis of ERS and ENVISAT InSAR data in northern Mojave, California: San Francisco, California, America Geophysical Union, 2010 Fall Meeting, abstract G42A–06.

Perroy, R.L., Bookhagen, B., Asner, G.P., and Chadwick, O.A., 2010, Comparison of gully erosion estimates using airborne and ground-based LiDAR on Santa Cruz Island, California: Geomorphology, v. 118, p. 288–300, doi:10.1016/j.geomorph.2010.01.009.

Petersen, M.D., Cao, T., Campbell, K.W., and Frankel, A.D., 2007, Time-independent and time-dependent seismic hazard assessment for the State of California: Uniform California Earthquake Rupture Forecast Model 1.0: Seismological Research Letters, v. 78, p. 99–109, doi:10.1785/gssrl.78.1.99.

Phillips, F.M., 2008, Geological and hydrological history of the paleo–Owens River drainage since the late Miocene, *in* Reheis, M.C., Hershler, R., and Miller, D.M., eds., Late Cenozoic Drainage History of the Southwestern Great Basin and Lower Colorado River Region: Geologic and Biotic Perspectives: Geological Society of America Special Paper 439, p. 115–150, doi:10.1130/2008.2439(06).

Pollitz, F.F., Peltzer, G., and Burgmann, R., 2000, Mobility of continental mantle: Evidence from postseismic geodetic observations following the 1992 Landers earthquake: Journal of Geophysical Research–Solid Earth, v. 105, no. B4, p. 8035–8054, doi:10.1029/1999JB900380.

Reheis, M.C., and Dixon, T.H., 1996, Kinematics of the Eastern California shear zone: Evidence for slip transfer from Owens and Saline Valley fault zones to Fish Lake Valley fault zone: Geology, v. 24, p. 339–342, doi:10.1130/0091-7613(1996)024<0339:KOTECS>2.3.CO;2.

Reheis, M.C., and Sawyer, T.L., 1997, Late Cenozoic history and slip rates of the Fish Lake Valley, Emigrant Peak, and Deep Springs fault zones, Nevada and California: Geological Society of America Bulletin, v. 109, p. 280–299, doi:10.1130/0016-7606(1997)109<0280:LCHASR>2.3.CO;2.

Renne, P.R., Balco, G., Ludwig, K.R., Mundil, R., and Min, K., 2011, Response to the comment by W.H. Schwarz et al. on "Joint determination of K-40 decay constants and Ar-40*/K-40 for the Fish Canyon sanidine standard, and improved accuracy for Ar-40/Ar-39 geochronology" by P.R. Renne et al. (2010): Geochimica et Cosmochimica Acta, v. 75, p. 5097–5100, doi:10.1016/j.gca.2011.06.021.

Rockwell, T.K., Lindvall, S., Herzberg, M., Murbach, D., Dawson, T., and Berger, G., 2000, Paleoseismology of the Johnson Valley, Kickapoo, and Homestead Valley faults: Clustering of earthquakes in the Eastern California shear zone: Bulletin of the Seismological Society of America, v. 90, p. 1200–1236, doi:10.1785/0119990023.

Rood, D.H., Hall, S., Guilderson, T.P., Finkel, R.C., and Brown, T.A., 2010, Challenges and opportunities in high-precision Be-10 measurements at CAMS: Nuclear Instruments & Methods in Physics Research, Section B, Beam Interactions with Materials and Atoms, v. 268, p. 730–732, doi:10.1016/j.nimb.2009.10.016.

Rood, D.H., Burbank, D.W., and Finkel, R.C., 2011, Chronology of glaciations in the Sierra Nevada, California, from ^{10}Be surface exposure dating: Quaternary Science Reviews, v. 30, p. 646–661, doi:10.1016/j.quascirev.2010.12.001.

Rood, D.H., Brown, T.A., Finkel, R.C., and Guilderson, T.P., 2013, Poisson and non-Poisson uncertainty estimations of ^{10}Be/^{9}Be measurements at LLNL-CAMS: Nuclear Instruments & Methods in Physics Research, Section B, Beam Interactions with Materials and Atoms, v. 294, p. 426–429, doi:10.1016/j.nimb.2012.08.039.

Roquemore, G., 1980, Structure, tectonics, and stress-field of the Coso Range, Inyo County, California: Journal of Geophysical Research, v. 85, p. 2434–2440, doi:10.1029/JB085iB05p02434.

Roquemore, G.R., 1981, Active Faults and Associated Tectonic Stress in the Coso Range, California [Ph.D. thesis]: Reno, Nevada, University of Nevada, 134 p.

Roquemore, G.R., and Zellmer, J.T., 1983, Ground cracking associated with the 1982 magnitude 5.2 Indian Wells Valley earthquake: California Geology, v. 36, p. 197–200.

Saint-Amand, P., 1987, Red Cinder Mountain and Fossil Falls, California, *in* Hill, M.L., ed., Geological Society of America Centennial Field Guide–Cordilleran Section, p. 43–44.

Sauber, J., Thatcher, W., Solomon, S.C., and Lisowski, M., 1994, Geodetic slip rate for the Eastern California shear zone and the recurrence time of Mojave Desert earthquakes: Nature, v. 367, p. 264–266, doi:10.1038/367264a0.

Savage, J.C., Lisowski, M., and Prescott, W.H., 1990, An apparent shear zone trending north-northwest across the Mojave Desert into Owens Valley, eastern California: Geophysical Research Letters, v. 17, p. 2113–2116, doi:10.1029/GL017i012p02113.

Shelef, E., and Oskin, M., 2010, Deformation processes adjacent to active faults: Examples from eastern California: Journal of Geophysical Research–Solid Earth, v. 115, B05308, doi:10.1029/2009JB006289.

Smith, G.I., and Street-Perrott, F.A., 1983, Pluvial lakes of the western United States, *in* Wright, H.E., and Porter, S.C., eds., Late-Quaternary Environments of the United States: Minneapolis, University of Minnesota Press, p. 190–212.

Stewart, J.H., 1988, Tectonics of the Walker Lane belt, western Great Basin: Mesozoic and Cenozoic deformation in a zone of shear, *in* Ernst, W.G., ed., Metamorphism and Crustal Evolution of the Western United States, Ruby Volume VII: Englewood Cliffs, New Jersey, Prentice Hall, p. 685–713.

Stone, J.O., 2000, Air pressure and cosmogenic isotope production: Journal of Geophysical Research, v. 105, p. 23,753–23,759, doi:10.1029/2000JB900181.

Stone, J.O., 2004, Extraction of Al and Be from Quartz for Isotopic Analysis: University of Washington Cosmogenic Nuclide Laboratory Methods and Procedures, 8 p., http://depts.washington.edu/cosmolab/chem/Al-26_Be-10.pdf (accessed July 2010).

Thompson, S.C., Weldon, R.J., Rubin, C.M., Abdrakhmatov, K., Molnar, P., and Berger, G.W., 2002, Late Quaternary slip rates across the central Tien Shan, Kyrgyzstan, Central Asia: Journal of Geophysical Research–Solid Earth and Planets, v. 107, 2203, doi:10.1029/2001JB000596.

Unruh, J., Hauksson, E., Monastero, F.C., Twiss, R.J., and Lewis, J.C., 2002, Seismotectonics of the Coso Range–Indian Wells Valley region, California: Transtensional deformation along the southeastern margin of the Sierran microplate, *in* Glazner, A.F., Walker, J.D., and Bartley, J.M., eds., Geologic Evolution of the Mojave Desert and Southwestern Basin and Range: Geological Society of America Memoir 195, p. 277–294.

Unruh, J., Humphrey, J., and Barron, A., 2003, Transtensional model for the Sierra Nevada frontal fault system, eastern California: Geology, v. 31, p. 327–330, doi:10.1130/0091-7613(2003)031<0327:TMFTSN>2.0.CO;2.

Wallace, R.E., 1968, Notes on stream channels offset by the San Andreas fault, southern Coast Ranges, California: Stanford University Publications in Geological Sciences, v. 11, p. 6–20.

Wesnousky, S.G., 2005, Active faulting in the Walker Lane: Tectonics, v. 24, p. 35, doi:10.1029/2004TC001645.

Whitmarsh, R.W., 1998, Geologic Map of the Coso Range: Boulder, Colorado, Geological Society of America Online Map Series, scale 1:24,000, doi:10.1130/1998-whitmarsh-coso.

Wills, C.J., 1989, Sierra Nevada Fault Zone–Haiwee Segment, Inyo County, California: California Division of Mines and Geology Fault Evaluation Report FER-208, scale 1:24,000, 2 sheets, 8 p. text.

Zehfuss, P., Bierman, P., Gillespie, A., Burke, R., and Caffee, M., 2001, Slip rates on the Fish Springs fault, Owens Valley, California, deduced from cosmogenic Be-10 and Al-26 and soil development on fan surfaces: Geological Society of America Bulletin, v. 113, p. 241–255, doi:10.1130/0016-7606(2001)113<0241:SROTFS>2.0.CO;2.

Zielke, O., and Arrowsmith, J.R., 2012, LaDiCaoz and LiDARimager-MATLAB GUIs for LiDAR data handling and lateral displacement measurement: Geosphere, v. 8, p. 206–221, doi:10.1130/GES00686.1.

Science Editor: Nancy Riggs
Associate Editor: Eric Kirby

Manuscript Received 6 October 2012
Revised Manuscript Received 5 March 2013
Manuscript Accepted 30 March 2013

Printed in the USA